Structural Performance Of 3D Printed Concrete Load Bearing Walls

STRUCTURAL PERFORMANCE OF 3D PRINTED CONCRETE

LOAD-BEARING WALLS

by

Arafat Abdulrahman Mohammed

A Thesis presented to the Faculty of the
American University of Sharjah
College of Engineering
In Partial Fulfillment
of the Requirements
for the Degree of

Master of Science in
Civil Engineering

Sharjah, United Arab Emirates

June 2024

Declaration of Authorship

I declare that this project/thesis/dissertation is my own work and, to the best of my knowledge and belief, it does not contain material published or written by a third party, except where permission has been obtained and/or appropriately cited through full and accurate referencing.

Signed Arafat Abdulrahman Mohammed

Date 11 / June / 2024

Approvals

We, the undersigned, approve the Masters Thesis written by: Arafat Mohammed

Thesis Title: Structural Performance Of 3D Printed Concrete Load Bearing Walls

Date of Defense: 11 / June / 2024

Name, Title and Affiliation	**Signature**
Dr. Adil Al-Tamimi Professor Department of Civil Engineering Thesis Advisor	
Dr. Tarig Ali Professor Department of Civil Engineering Thesis Examiner (Internal	
Dr. Zied Bahroun Professor Department of Industrial Engineering Thesis Examiner (External)	

Accepted by:

Dr. Fadi Aloul
Dean
College of Engineering

Dr. Mohamed El-Tarhuni
Vice Provost for Research and Graduate Studies Office of
Research and Graduate Studies

Acknowledgments

My sincere gratitude goes out to my adviser, Prof. Adil K. Al-Tamimi, for his invaluable guidance, great advice, support, and mentorship throughout the duration of this research. His expertise and knowledge in the field of 3D concrete printing have been instrumental in shaping the direction and success of this work. I am deeply grateful for his unstopped support and motivation, which have significantly contributed to the accomplishments of this research. His encouragement has not only shaped my research skills but also advanced my professional growth. My profound thanks to him for his exceptional contribution and dedicated mentorship.

I am also deeply grateful to Concretive Company for their collaboration and support in providing access to their cutting-edge 3D concrete printing technology and resources. Their commitment to advancing construction practices through innovation has been a driving force behind the progress of this study. I sincerely appreciate their assistance in facilitating and printing the walls, which has been crucial for the experimental phase of this research.

I want to sincerely thank each and every one of the instructors in the Civil Engineering Department who have guided me during my graduate studies. My academic experience has been greatly influenced by their commitment to teaching and vast knowledge. I have gained a solid foundation and a thorough understanding of numerous civil engineering principles from each course, which have been essential to the accomplishment of this project.

I would like also to express my heartfelt gratitude to the American University of Sharjah for granting me the master's scholarship, which has been pivotal in my academic and professional development. I am also thankful for the supportive environment, as well as the opportunities provided through the teaching assistantship and research assistantship roles, which have greatly enhanced my knowledge and skills.

Dedication

In the name of Allah, the Most Gracious, the Most Merciful.

In the spirit of the Prophet Mohammad, peace be upon him, whose timeless teachings continue to illuminate my path and guide my every step.

To my beloved parents, whose unwavering love and support have been my foundation. To my dear father, who departed this world before he could witness the fulfillment of the dream he so unforgettable for me—your pride in me has been my strength.

To my invaluable sister and brothers, whose encouragement and belief in my abilities have been a constant source of motivation.

To my valued friends, both in my homeland and in my second home, the UAE, and to those scattered across the globe, your friendship and support have been a beacon of light in my journey.

To all of humanity, whose collective spirit inspires me to contribute to a better world.

Arafat

Abstract

Modern construction techniques have evolved in recent years with the introduction of 3D Concrete Printing (3DCP) technology. This innovative digital construction approach offers rapid, cost-effective, and sustainability solutions. The 3DCP walls used as load-bearing walls are an essential component and the primary section of the 3D printed constructions. Therefore, this study investigates the behavior of large-scale 3DCP walls under axial loading to evaluate their load-bearing capacity. The used mix consists of optimized materials, including glass fibers (GF) for reinforcement, enhancing mechanical properties, and crack resistance. Rheological testing ensured the mix's quality and efficiency, assessing properties like extrudability, flowability, and buildability. Mechanical tests confirmed the mix as high-strength concrete with an 85 MPa compressive strength. Uniform axial compression loading tests were conducted to analyze the structural behavior, deformation, and crack patterns of 3DCP load-bearing walls with different cross-section configurations. The walls were categorized into two types: gapped walls, which include GLBW-3T (three-truss gapped wall), GLBW-4T (four-truss gapped wall), and GLBW-5T (five-truss gapped wall), and a solid wall, SLBW, which is a fully solid section designed to achieve maximum load-bearing capacity. In this study, materials consumption was a key factor in identifying the optimal and economical structural efficiency. The SLBW exhibited the highest resistance to cracking with a crack load-to-volume ratio of 4.02 N/cm^3. Conversely, GLBW-3T and GLBW-5T, both featuring gapped sections with varying truss configurations, showed similar efficiency with crack load-to-volume ratios of 3.12 N/cm^3 and 3.04 N/cm^3, respectively. GLBW-4T demonstrated the least efficient performance, with a crack load-to-volume ratio of 2.48 N/cm^3. Moreover, the crack pattern intensity and structural stability were highest in the SLBW, followed by the GLBW-3T, while, the GLBW-5T performed the least favorably. This study underscores the superior structural performance and material efficiency of the GLBW-3T configuration, achieving an optimal balance of material use and structural integrity.

Keywords: 3D concrete printing (3DCP), Digital construction, Composite materials, Concrete rheology, Mechanical testing, Structural performance, failure mode, cracks pattern, Solid load-bearing wall (SLBW), Gaped load-bearing wall (GLBW).

Table of Contents

List of Figures

List of Tables

List of Abbreviations

3DCP 3D Concrete Printing

ACI - American Concrete Institute

AMC - Additive Manufacturing Construction

ASTM - American Society for Testing and Materials

CAD - Computer-Aided Design

CC - Contour Crafting

ECC - Engineered Cementitious Composites

ESL - Extrusion-based Systems with Layering

FDM - Fused Deposition Modeling

FEM - Finite Element Method

FRC - Fiber Reinforced Concrete

FRP - Fiber-Reinforced Polymer

GGBFS - Ground Granulated Blast Furnace Slag

ICC-ES - International Code Council Evaluation Service.

LBW - Load-Bearing Wall

OPC - Ordinary Portland Cement

QA/QC - Quality Assurance/Quality Control

RC - Reinforced Concrete

Chapter 1. Introduction

1.1 Background & Motivation

Three-Dimensional Concrete Printing (3DCP) is an emerging technology that combines digital technologies and new insights from materials technologies to allow free-form construction without the use of formwork. 3DCP is an additive manufacturing technique where the construction is conducted through layer-by-layer addition of material. It has the potential to revolutionize the construction industry. This innovative technology refers to an automated additive manufacturing of cementitious layers that allows for the creation of complex, custom-designed structures using a layering process that builds up the structure one layer at a time. The structural performance of 3D-printed concrete elements depends on several factors, including the properties of the concrete material, the design of the structure, and the printing process itself. In general, 3D-printed concrete structures have been found to have good structural performance and are capable of supporting significant loads. One of the main advantages of 3D-printed concrete structures is their ability to be designed and fabricated with a high degree of customization. This allows for the creation of structures with complex geometries and internal structures that would be difficult or impossible to create using traditional construction methods. However, there are still many challenges that need to be overcome to fully realize the potential of 3D concrete printing. Further research and development are needed to improve the strength, durability, and other properties of 3D-printed concrete structures and optimize the printing process.

3D concrete printing is a construction technology that involves the use of a large-scale 3D printer to create three-dimensional structures and objects out of concrete. This technology is gaining popularity in the construction industry due to its ability to create complex geometries quickly and efficiently, as well as its potential to reduce material waste and labor costs. The process of 3D concrete printing typically involves the use of a robotic arm or gantry system that is programmed to extrude layers of concrete based on a digital model. The printer head moves along a pre-determined path, depositing the concrete material layer-by-layer until the desired object is formed. Depending on the printer and its capabilities, the process can take anywhere from several hours to several days to complete. There are a variety of concrete materials that can be used in 3D printing, including traditional Portland cement, as well as more specialized formulations like high-performance concrete and fiber-reinforced concrete. These materials can be customized to meet specific design requirements, such as strength, durability, and sustainability. Additionally, it offers significant environmental advantages, including the utilization of waste materials such as industrial by-products like silica fume, fly ash, and ground granulated blast slag as cement replacements. It also reduces material waste by using almost the exact amount of concrete needed for the structure, thus minimizing excess. Furthermore, it decreases carbon emissions associated with transportation and construction operations. As technology continues to advance, it has the potential to transform construction methodology, making it faster, more efficient, and more sustainable.

Even though it is generally acknowledged that the next industrial revolution includes the total automation of 3DCP, it is thought that 3DP cementitious materials technology has reached maturity at this point. Unfortunately, there are many difficulties to overcome, and still no global consensus on the main needs, material selection, mix design technique, and the assessment criteria of cementitious material fresh and hardened qualities [1], [2]. A large number of trial-and-error attempts and conservative designs, particularly for structural aspects, are present alongside the current 3DCP applications. This is because 3DCP research has not advanced at a rate that keeps up with the construction industry's interest in lowering labor costs and raising productivity [3]. Thus, there is an obvious need for more investigations to analyze the problems and fill the research gaps. In addition to that, there is a shortage of structural performance investigation in terms of failure modes of structural elements. As is evident in the industry, the application of 3DCP is often combined with traditional reinforced concrete elements. For example, many constructed 3DCP buildings worldwide were established as conventional reinforced concrete members including slabs, beams, columns, and footings, and the printed parts represent the wall partitions that only resist their own weight.

1.1.1 Load-bearing wall overview

Load-bearing 3D printed walls refer to walls constructed using 3D printing technology capable of supporting structural loads. These structural elements are engineered to withstand the forces imposed on them, such as vertical loads (gravity), lateral loads (wind), and seismic forces. The design process involves considering factors like wall thickness, reinforcement placement, and structural connections. To enhance the structural integrity, reinforcement elements like steel bars or fibers may be incorporated into the 3D-printed walls during the printing process. Therefore, reinforcements help to distribute the load and increase the wall's ductility and strength. However, according to a study conducted by Han, et al., “The use of horizontal steel reinforcement reduces the ultimate bearing capacity of 3D printed concrete walls under axial compression. Emphasizing that, The layers in which the horizontal steel reinforcement is set are weak zones” [4]. Whereas, the use of fiber reinforcement enhances the compressive capacity of the walls in terms of ductility and macrocracks control. Moreover, test load-bearing 3D printed walls undergo rigorous testing and evaluation to ensure their compliance with structural regulations and building codes. Typically, structural engineers analyze the walls' strength, durability, and overall performance to verify their load-bearing capacity. While load-bearing 3D printed walls have shown great potential, their adoption is still in the early stages, and further research, development, and testing are needed before they become widely implemented in the construction industry. In this proposed study, plain walls with different truss-type core patterns (triangular) will be assessed to explore the performance of the walls under gravity loads. To examine the structural performance of the system, four large-scale 3D-printed walls were tested under axial compression to analyze deformation, crack patterns, and failure modes and behaviors.

1.2 Research Objectives

The primary aim of this study is to conduct an experimental investigation to assess the feasibility of using a 3D-printed concrete wall as a load-bearing structural element. Also. the research objectives of 3D concrete printing (3DCP) load-bearing walls intented to explore and address various aspects of this innovative construction technology. These objectives are designed to improve the understanding, performance, and application of load-bearing walls constructed using 3DCP. The project objectives are to:

- Assessing the fresh properties of the mix design, including slump-flow-table, extrudability, buildability, and the setting time.
- Evaluating the mechanical behavior of printed specimens, including compressive, tensile, and flexural strengths, to determine stress-strain characteristics.

- Investigating the load-bearing capacity of 3D-printed concrete walls under axial compression.
- Analyzing the structural performance of large-scale 3DCP walls under axial compressive loads to determine performance, cracking patterns, and failure mechanisms.

1.3 Research Significance & Problem Statement

During construction, reconstruction, and demolition, tons of non-biodegradable and industrial wastes are generated every year. Dirty landfills, high transportation ,costs and environmental issues of such materials have forced worldwide researchers to find a green solution to deal withsuch wastes. Furthermore, the revolution of automation, technologies, and the efficient productivity of available machined learning projects has led the construction industry to look for innovations. One such innovation is using 3D concrete printing known as manufacturing additive construction (MAC). Powerful analysis tools, energy-efficient robotics, and advanced technological developments have enabled alternate use of conventional to 3D-printed buildings. Despite the conventional use of materials like cement and steel in construction, detailed design studies are conducted worldwide to prove the efficiency of 3DCP structures in terms of cost, performance, weight, and productivity. The proposed 3DCP construction not only gives a safe, economical, and environmentally friendly design but also helps to get rid of huge waste produced during conventional concrete construction. While significant progress has been made in 3DCP applications in recent years, challenges remain, particularly in building fully 3D-printed structures due to the lack of standard provisions. Given that walls play a critical role as load-bearing elements in 3DCP structures, understanding their load-bearing capacity is essential for designing efficient and resilient structures. Addressing the existing research gap on the structural behavior of 3DCP load-bearing walls, this study aims to print and test structural walls to evaluate their load-bearing capacity. A mix design optimized to meet rheological and buildability requirements was employed, and the failure mode of the load-bearing walls was determined through axial compressive load testing.

1.4 Contemporary Issues & Project Constraints

Every research endeavor encounters challenges throughout its various phases, from sourcing scholarly materials to experimental execution. Notably, the absence of established 3DPC building codes for load-bearing walls underscores the importance of staying updated on literature and code developments. Overcoming the barrier of printing large-scale elements required seeking alternatives and eventually collaborating with a 3D printing company for wall production in this study. However, addressing contemporary issues and constraints is imperative for the widespread acceptance and effective implementation of 3DCP load-bearing walls:

- Research and standardization efforts are needed to develop suitable 3DCP materials that meet relevant industry standards required for 3DCP wall construction.
- Availability of suitable printing materials and their associated costs can impact the feasibility of 3DCP projects. Procuring high-quality materials at affordable prices is essential for project viability.
- In terms of strength and durability, material optimization, proper curing, and quality control are essential in addressing this constraint.
- Developing and updating design codes and guidelines specific to 3DCP load-bearing walls is crucial to ensure their structural integrity and compliance with safety standards.
- Implementing quality control measures during the 3D printing process to monitor material properties, layer bonding, and overall structural integrity is essential. Regular inspections and testing are necessary to identify potential defects or weaknesses in the walls.
- Scaling up 3DCP technology for large-scale load-bearing wall construction presents challenges in terms of printing speed, equipment capabilities, and material logistics.
- Incorporating reinforcement within 3DCP load-bearing walls, such as steel or fiber reinforcement, is important for enhancing structural strength and controlling cracks. Developing effective reinforcement methods for 3DCP construction is an ongoing area of research.

Chapter 2. Literature Review

2.1 Historical Background of 3-D Concrete Printing

Construction automation and robotics, which are not new to the sector, are where 3-D printing in construction first emerged. The building materials (concrete, mortar, asphalt, etc.) act as the printer's ink, and the mobile or stationary system is made up of various robotic subsystems or components. To print a digital image on paper using a desktop printer, a computer must send the digital image to the printer. Similar to this, while building a facility, the intention is to send a digital model to the printer to build it above, below, or both positions. Over the past ten years, concrete additive manufacturing (AM) technologies - often referred to as cement-based 3D printing - have grown rapidly, proving their capacity to simplify the construction industry. Concrete additive manufacturing (AM) can quickly and affordably produce high-precision construction components [5]. The amount of labor needed can be reduced as a result. The majority of AM solutions in the construction industry use an extrusion-based material approach based on sliced CAD geometry to create concrete layers [6]. Using this technique, complex shapes can be built more freely as traditional plywood concrete molds are not required. Concrete AM can be done either in situ or as a prefabricated part. In-situ 3D printing concrete is frequently used to create building walls as seen by the BOD building by COBOD in Denmark, Studio 2030 by CyBe in Saudi Arabia, and the Dubai Municipality building by ApisCore in the UAE [7]. These examples simply serve as indications of what is possible. Yet, there is an obvious mismatch between building codes and AM technology, calling for a method to fulfill the structural regulation requirement.

2.2 Extrusion-Based Methods for Additive Manufacturing

Concrete extrusion is the most explored large-scale 3DCP technique. Typically, a stiff, viscoplastic, cement-based print material is pressurized and squeezed through a nozzle that is digitally controlled to continuously move and print the concrete filaments to build a structure [8]. Although, extrusion-based 3DCP can have massive benefits to the construction sector, however, the optimization of the mix still requires more investigations due to the high-cement content of the current mix design, which is necessary for improving the rheology of the paste and setting time [9], [10]. To date, the paradoxical hardest step in the mix design is the optimization of extrudability and buildability, which means, it is hard to balance between flowability and fresh plastic strength [11]. Contour crafting is the common method for large-scale 3DCP, however, other methods such as concrete printing, functionally graded 3DCP, and ultra-high performance 3DCP, have also been introduced [12].

2.2.1 Contour crafting

In the mid-1990s, a technology named "Contour Crafting" raised, which is an innovative 3D concrete printing technology developed by Dr. Behrokh Khoshnevis at the University of Southern California. The technology was later patented in 2010 [13]. This technology initially started as a ceramic paste extrusion method [14], but was later expanded to cementitious materials, aiming at large-scale structural elements and even the entire facility. It is a large-scale robotic construction method that has the potential to revolutionize the field of architecture and construction. The basic elements of this technology include a concrete tank, a hose, a pumping mechanism, a nozzle, and a robotic arm that guides the nozzle in x, y, and z directions. The nozzle deposits the concrete layer by layer, and the concrete layers cure and gain sufficient strength fast enough to support the new layers above them [15]. The key features and principles of Contour Crafting include:

- Gantry System: Contour Crafting utilizes a gantry system, which is a large-scale robotic arm or framework that moves along a predefined path. The gantry system is equipped with an extrusion nozzle that deposits layers of concrete to construct the desired structure.
- Layer-by-Layer Construction: Similar to other 3D concrete printing methods, Contour Crafting builds structures layer by layer. The robotic arm moves along the predefined path while extruding a specially formulated concrete mixture, following the design instructions provided by a computer program.
- Integration of Multiple Functions: Contour Crafting is designed to integrate various construction functions into a single system. This includes tasks such as concrete deposition, reinforcement installation, plumbing, electrical wiring, and even the provision for finishing touches like applying paint or adding texture.
- Rapid Construction: Contour Crafting has the potential to significantly accelerate the construction process. By automating construction tasks and eliminating the need for manual labor, it can build structures at a faster pace compared to traditional construction methods.

2.2.2 Selective aggregation

Midway through the 1990s, "Selective Aggregation," another additive or layered manufacturing method, was introduced. This method involved first laying down a sand (silica) matrix, then selectively depositing cement on the sand matrix, and finally activating the cement binder with steam [15]. Using computer-aided design and analytical modeling tools, the procedure produced a robust and dense material that could be mechanized [16]. Selective aggregation techniques can be implemented using various methods and materials, depending on the specific technology and application. Those methods include Selective Laser Sintering (SLS), Binder Jetting, Drop-on-Demand Printing, and Aerosol Jet Printing. These methods offer advantages such as the ability to create complex geometries, the potential for multi-material printing, and the flexibility to incorporate different materials with varying properties into a single object. These techniques have applications in various industries, including aerospace, automotive, healthcare, and consumer products, where customized and highly functional components are required.

2.2.3 Concrete printing

Another popular large-scale 3D printing technique was concrete printing, which was developed by researchers at Loughborough University during the first decade of the twenty-first century. The concrete printing machine is composed of a 5.4 m 4.4 m 5.4 m frame and a movable horizontal beam that moves in the y and z dimensions while the printing head only moves in the x direction [17]. This method's nozzle can print both large areas and small details at various resolutions. This technology stood out from others since it concentrated on expanding the use of additive manufacturing in buildings for large-scale structural components. Additionally, the technique improved the functionality of the building's acoustic, thermal, and ventilation systems [18], [19].

2.2.4 Advances in Equipment

Until now, gantry-style and robotic concrete 3-D printers have both been effectively used in both academic and practical settings. In contrast to robotic arms, which frequently have a set dimension, gantry-style printers can be easily scaled up in size. A four-axis gantry printer may not be able to accomplish many complicated geometries, but a six-axis robot's speed and degrees of freedom make this possible [20]. A gantry-style printer often has a higher payload than a robotic arm.

The primary parts of a medium-sized four-axis gantry system are depicted in Figure 2.1 at NASA's Marshall Space Flight Center in Huntsville, Alabama, in the United States [15]. A gantry-type printer typically consists of a concrete deposition system, a concrete mixing and delivery system, and a gantry mobility system for x, y, and z positioning. Gantry printers come in a variety of sizes that range from small tabletop lab models to big-scale printers that can produce full-size building components as shown in Figure 2.2. A large-scale concrete 3-D printer with a four-axis gantry robot and an adjustable printing area of around 9 m by 4.5 m by 2.8 m was developed by the Eindhoven University of Technology (TU/e) in the Netherlands [21].

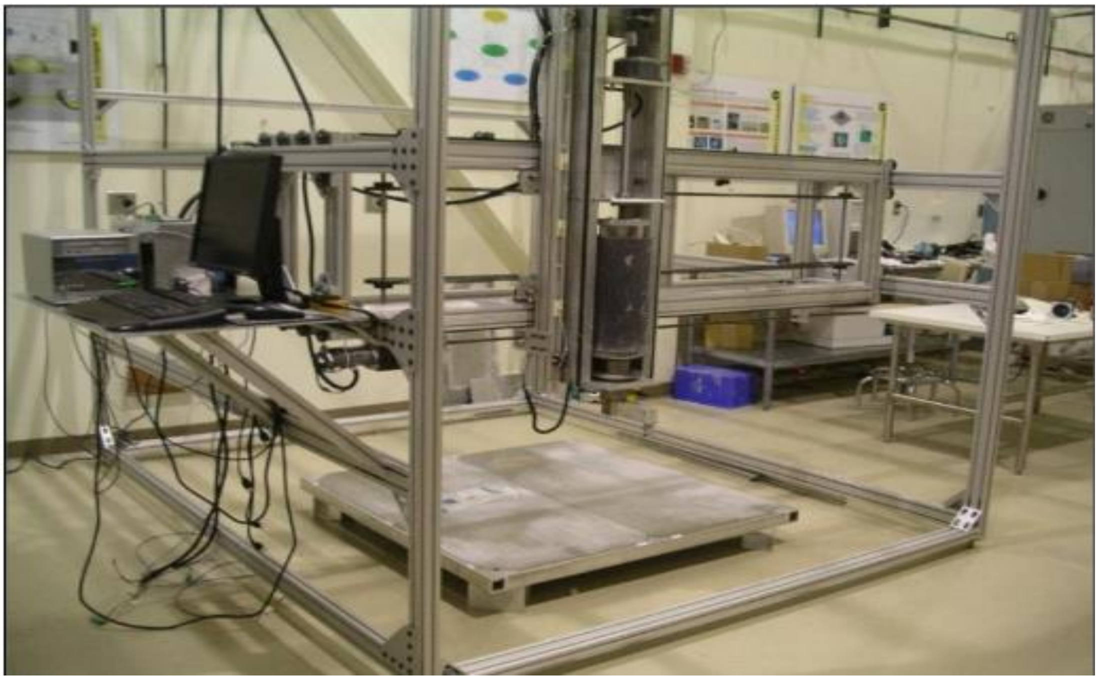

Figure 2.1 Gantry-style concrete 3-D printer at NASA's Marshall Space Flight Center [15].

Despite being successful in scaling up additive manufacturing for construction, gantry-style concrete 3-D printers still have considerable drawbacks. Gantry-style printers are typically restricted to vertical extrusion. Therefore, gantry-style printers produce 2.5-D topologies rather than real 3-D topologies. Robotic arms - illustrated in Figure 2.3, Figure 2.4 & Figure 2.5 - have been created as a way to carry out large-scale 3-D printing research and development to solve this problem. Printing complicated artifacts is made possible by the use of industrial robots equipped with programmable software and scripting languages, which greatly simplify planning and controlling robotic trajectories [22].

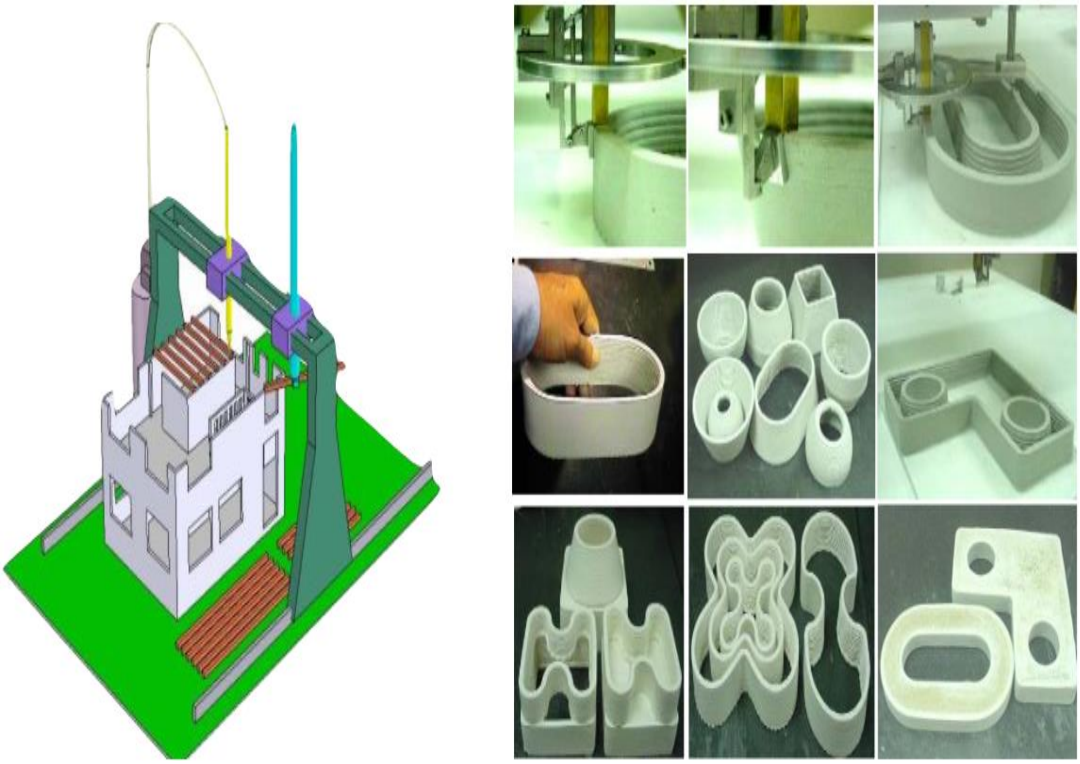

Figure 2.2 Initial Contour Crafting system to the (Left), and first realization attempts of 2.5D printed concrete shapes using CC [23].

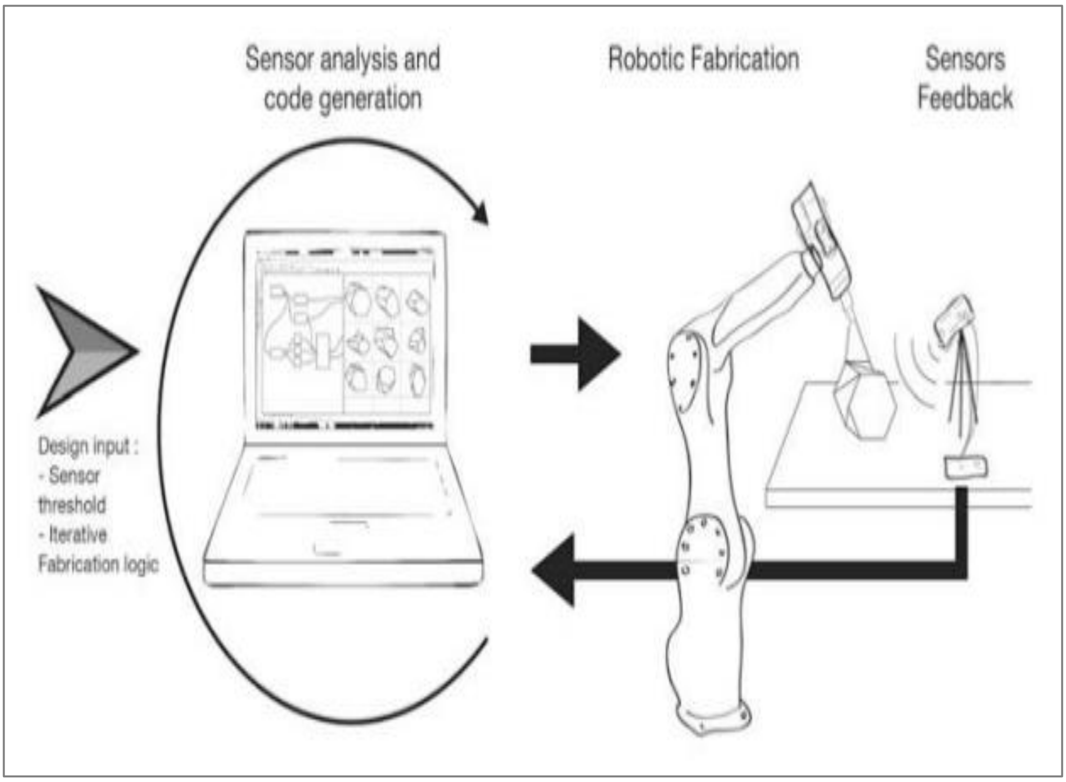

Figure 2.3 3D-printing workflow of robotic arm [23].

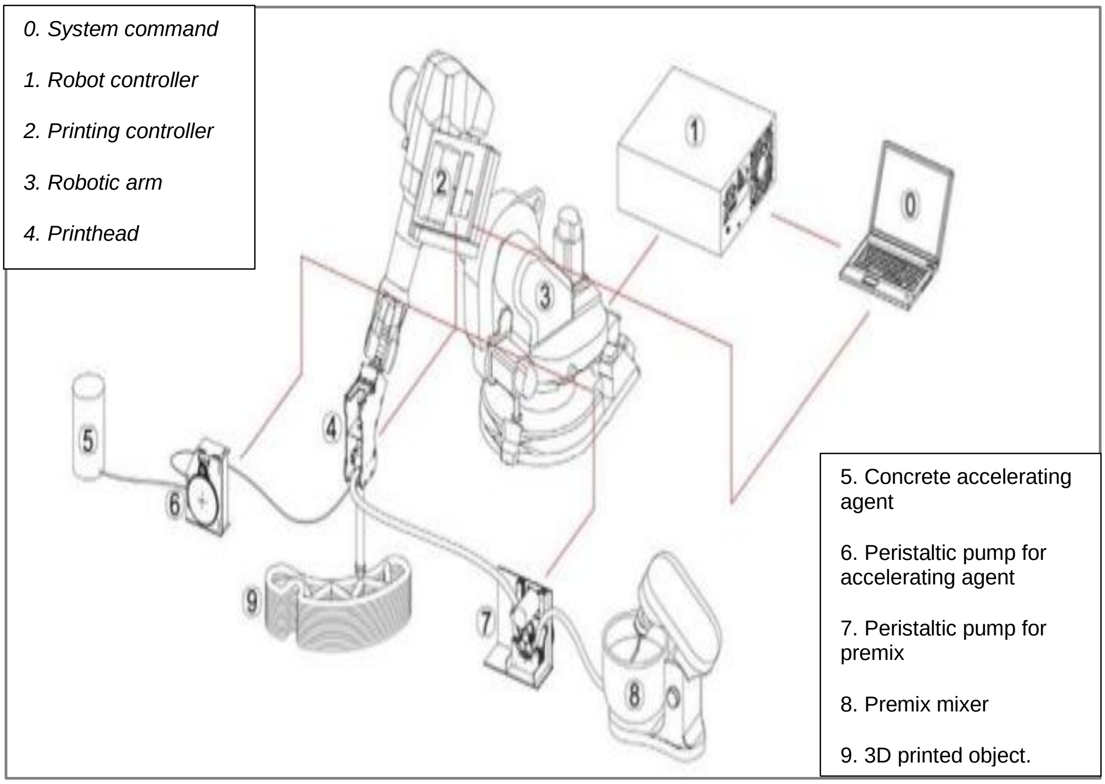

Figure 2.4 3D-printing components [23].

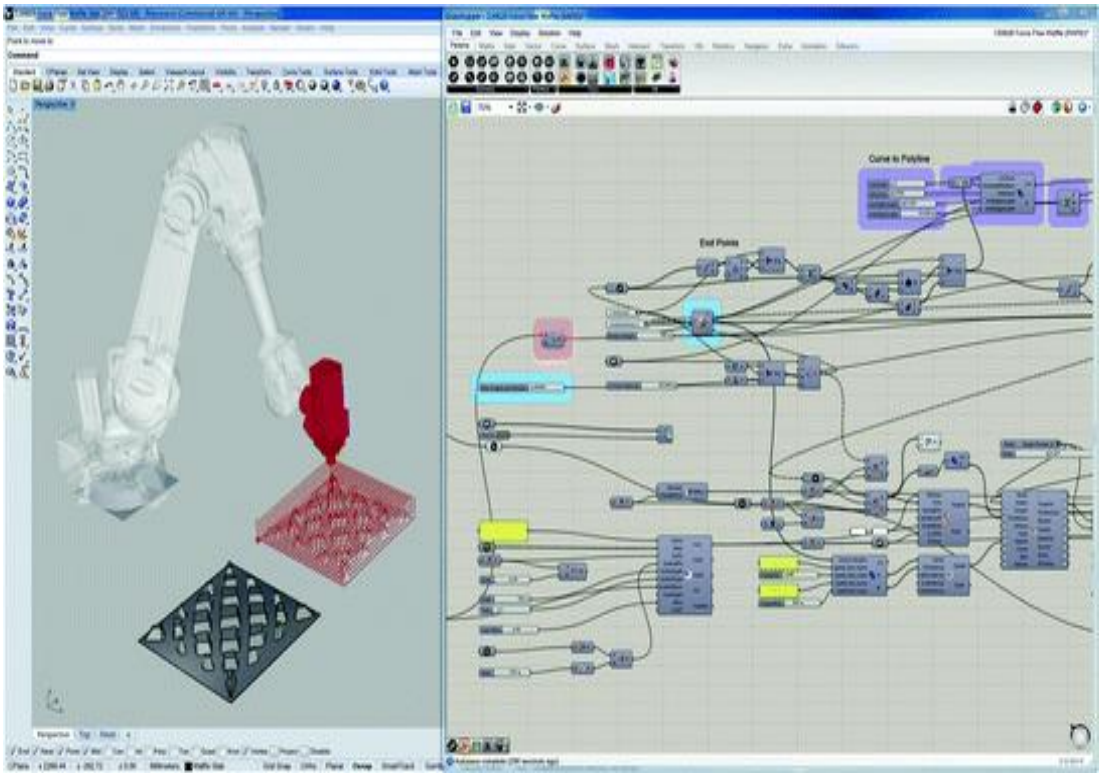

Figure 2.5 Grasshopper plugin for simulating robotic trajectories translated from a CAD model [23]

2.3 Literature Review on 3DPC Wall Structure

2.3.1 Structural performance of 3DPC walls in the early age during printing

Research done by (A.S.J. Suiker., 2018) presented a mechanistic model for analyzing and optimizing the mechanical performance of straight wall structures during 3D printing processes. The model distinguishes between failure by elastic buckling and plastic collapse, and the results are summarized in design graphs and failure mechanism maps as shown in Figure 2.6. The numerical results for three basic configurations, i.e., the free wall, the simply-supported wall, and the fully-clamped wall, printed under either linear curing or exponential curing, are demonstrated. Overall, this study provides valuable insights into the mechanical performance of 3D-printed walls. Based on his research, the simply-supported wall provides a lower bound for the wall buckling length, corresponding to the global buckling of the complete wall structure, while the fully-clamped wall gives an upper bound, reflecting the local buckling of an individual wall. The range of critical buckling lengths defined by these bounds may be further narrowed by the critical wall length for plastic collapse. For arbitrary wall configurations, an accurate model prediction for the critical buckling length and corresponding buckling mode can be obtained by deriving an expression for the non-uniform rotational stiffness provided by the support structure of a buckling wall. This has been demonstrated for a rectangular wall layout, which has proven to give a good agreement with the experimental buckling response [24].

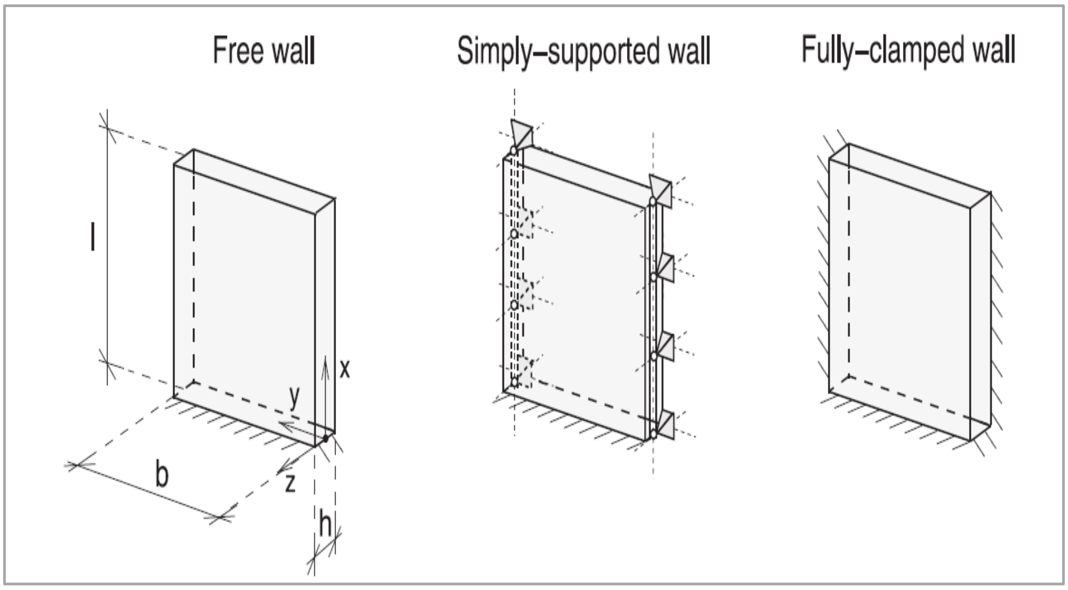

Figure 2.6 Three basic wall configurations: a free wall (left), a simply-supported wall (middle), and a fully-clamped wall (right) [24].

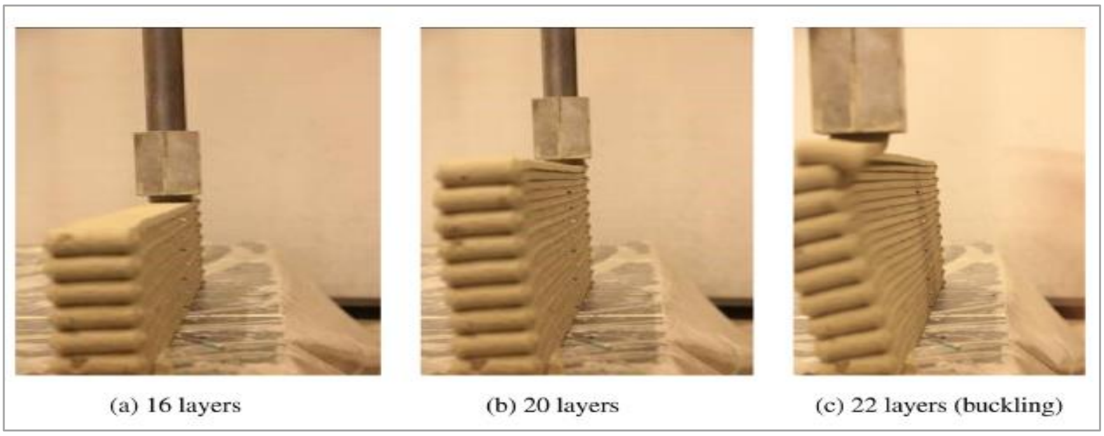

Figure 2.7 Free wall after the printing of 16 layers (a), 20 layers (b), and 22 layers, leading to buckling (c) [24].

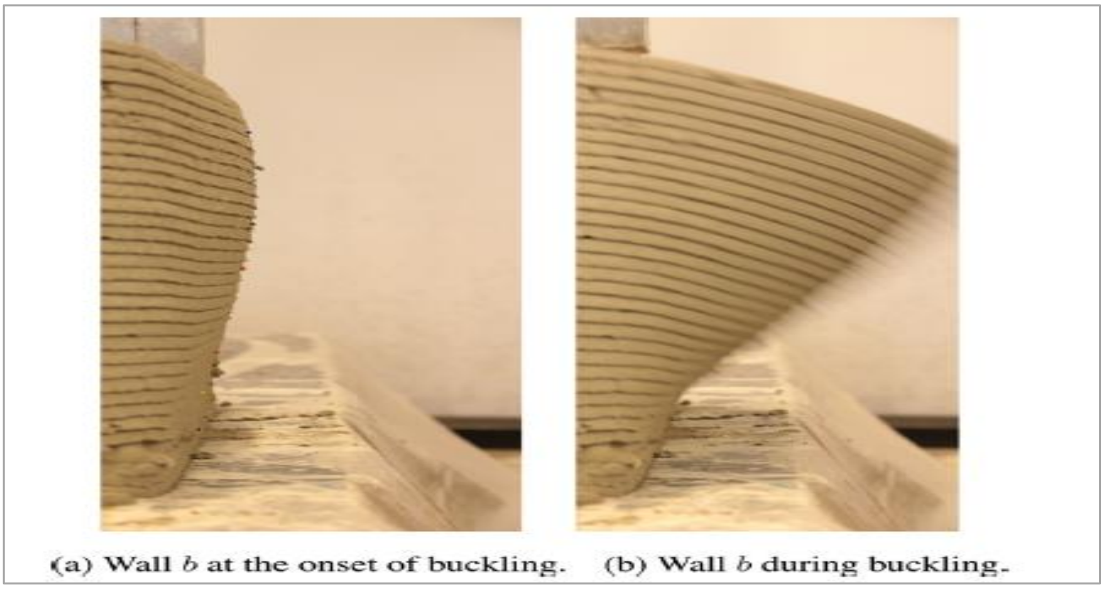

Figure 2.8 Rectangular wall lay-out of b = 625 mm and d = 250 mm after the printing of 33 layers. Deflection of wall b at the onset of buckling (a), and during buckling (b) [24].

(Kontovourkis & Tryfonos., 2020) published a paper that initially illustrates the development of a parametric-integrated algorithm for toolpath planning and 3DP control using an industrial robot, capable of being universally adjusted based on open-source extruders with small, medium, and large nozzle diameters as illustrated in Figure 2.9. In their study, earth, and clay-based materials are chosen because of their lower environmental impact and recyclability compared to concrete-based materials. Secondly, important printing parameters for toolpath planning, robotic and nozzle control, as well as robotic printing time, are presented and discussed in detail through 3DP experimental tests and a nonconventional wall study. The correlation of parameters in the early stage of design allows the assessment of their effectiveness to be used in the construction scale of non-conventional geometries towards minimization of 3DP time performance.

They have concluded that the application of earth or clay-based materials that could similarly contribute towards construction time reduction while offering lower environmental impact solutions and recyclability of applied material mixtures had been the object of research in several studies. Applications have been found in different projects, ranging from small to large structures by using different 3DP techniques. Moreover, the parametric investigation leads to a thorough and clear understanding of the effectiveness of the process to be used for the 3DP development of non-conventional shapes as opposed to conventional ones. On the one hand, the selection of specific 3DP parameters can maximize construction time performance by setting values in a way that balances layer height, outside wall thickness, infill density, nozzle diameter, and extrusion velocity can be achieved. On the other hand, a comparison between non-conventional and conventional 3DP shows that 3DP exhibits great advantages in terms of construction time and cost, more in the direction of 3DP of complex shapes since research has shown that the application of technology does not bring any dramatic increase in 3DP time performance if the comparison is made between non-conventional and conventional structures [25].

Figure 2.9 3D printing of brick unit no.1 derived from non-conventional wall with the largest overhang angle at 26.13o and with the application of 3×5 hex grid infill [25].

(Nguyen-Van et al., 2022) conducted a study on 3D concrete printing modeling of thin-walled structures [26]. Their article discusses the common failures encountered in 3D concrete printing and how they can be prevented. It also explains how finite element modeling can help predict the behavior of thin-walled structures during the printing process. The study uses early-age mechanical properties of two printable mixes as input data for the simulation and validates the finite element modeling by comparing it with 3DCP experiments of a hollow cylinder. The article concludes by discussing key parameters that affect the quality and performance of 3D-printed concrete and how they can be optimized. According to the research, The effect of extrusion width and mesh size on the buildability was carried out by modeling a straight thin-walled structure. The case study indicated that better constructability could be achieved by printing the thin wall with a larger extrusion width. This could be ascribed to the influence of the critical buckling length for the thin-walled structure, which is related to the stabilization of the print object during the 3DCP process.

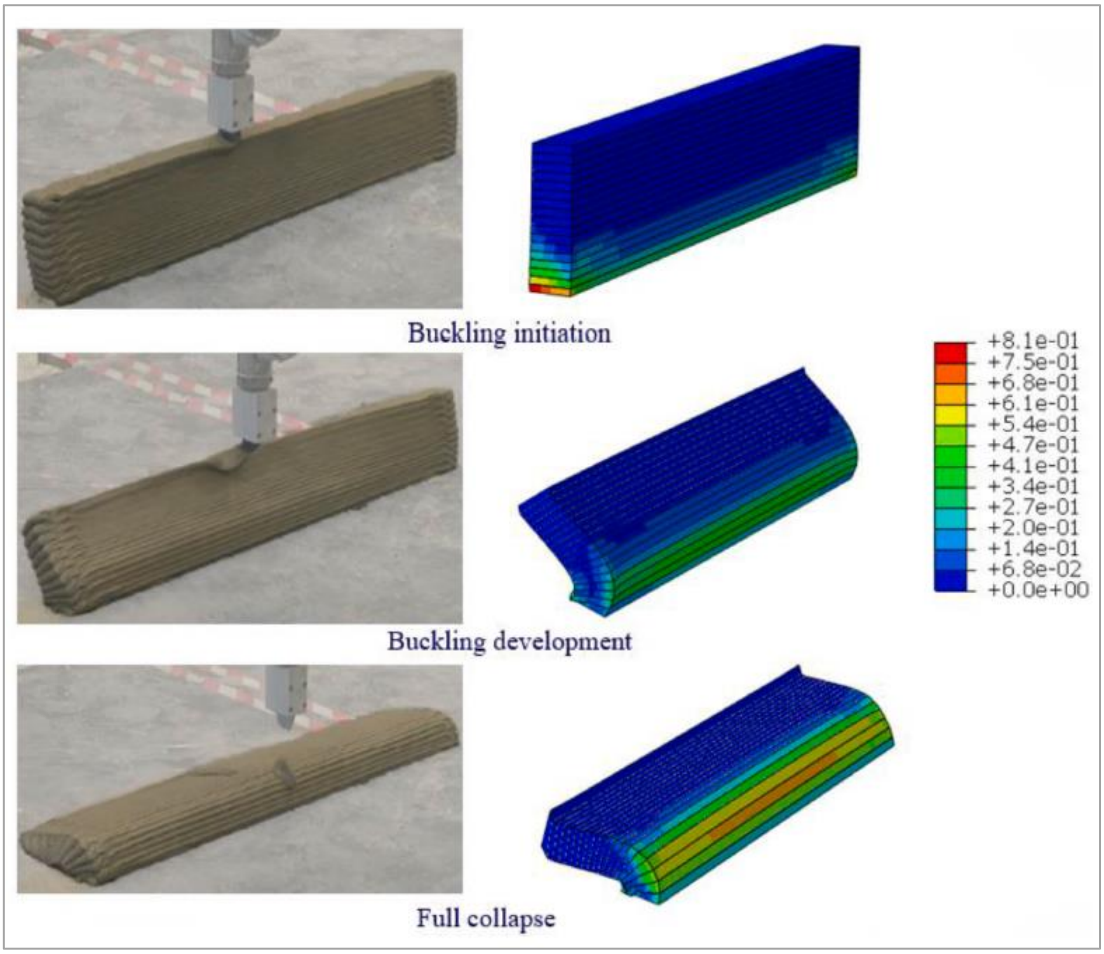

Figure 2.10 Buckling response comparison between experimental and numerical results of the 60 mm-thick wall structure (colors represent the maximum principal plastic strain distribution)[26].

Besides, a sensible mesh strategy can provide more accurate results than a uniform mesh size. Moreover, the FE model was able to reasonably predict either the point of failure (number of layers) or the two common modes of failure (elastic buckling and plastic collapse) in the 3DCP process as shown in Figure 2.10 and Figure 2.11. In addition, the numerical outcomes show a good agreement with the experimental outcomes. The numerical approach in this study provides a considerable improvement in illustrating and predicting the failure modes in comparison with other existing works. A shorter time step, together with a smaller element segment in 3DCP simulation, demonstrated that the numerical analysis could be asymptotic with the experimental results. Furthermore, it is deemed suitable to take the hardening speed of printing materials into the analysis [26].

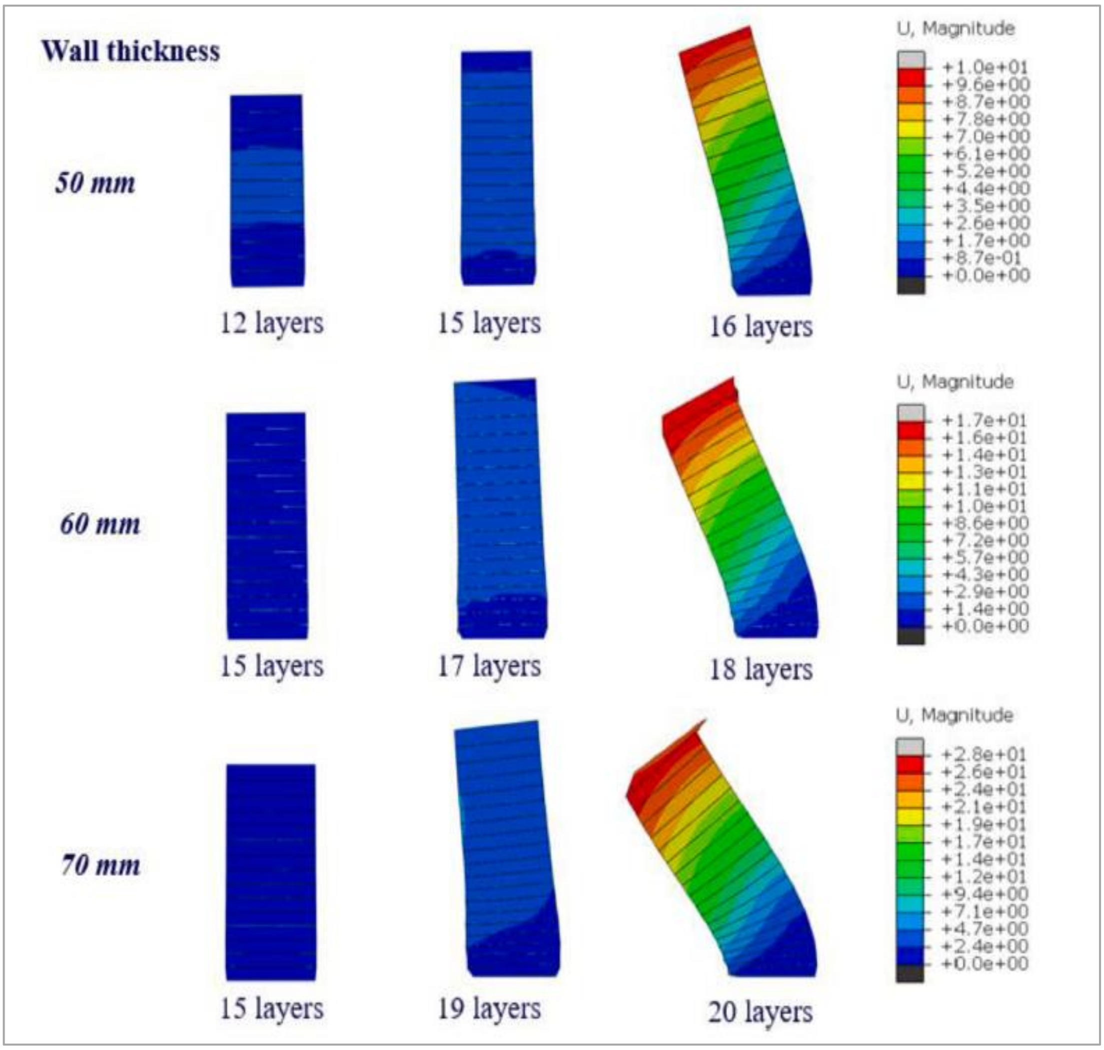

Figure 2.11 Cross-section deformations of the straight thin-walled structure at three moments (before failure, start failure, and during failure), printed by different extrusion widths, i.e., 50 mm, 60 mm, 70 mm (colors represent the relative magnitude of the display) [26].

2.3.2 Structural performance of 3DCP walls under uniaxial compression (load-bearing walls)

(Daungwilailuk et al. 2021.) conducted an experiment on large-scale 3D-printed concrete walls subjected to uniaxial load testing. The experiment involved two different wall patterns: flat and diamond walls. As illustrated in Figure 2.13, the strain and deflection of the walls under loading were experimentally monitored and recorded. Moreover, the finite-element method was carried out by ANSYS software to analyze the behavior of these walls with the assumption of linear elastic behavior. According to their experimental results the following conclusions are drawn [27]:

- Although 3D-printed concrete technology allows flexible architectural design for wall structures, the pattern and layout of the wall surface affect the performance of the structural elements. In this study, the diamond wall specimen exhibited a risk of failure owing to its waving shape. The pits of the diamond pattern exhibited large tensile strains, which resulted in concrete spalling and cracking. Therefore, it is necessary to consider the pattern of the wall surface in 3D-printed concrete.
- The study indicates that the inner truss inside 3D-printed concrete plays a role in the wall bracing. It can mitigate the wall bowing and prevent the buckling failure of the wall.
- The strain-gauge measurement results indicated that the different types of strain can occur in the same direction on the same wall surface. Additionally, the strain switched from tensile to compressive underloading. This was due to the wall bowing and the shape of the printed concrete.
- The finite-element analysis results for the strain agreed well with the experimental results. The analysis results for the tensile stress occurring in the wall model was approximated.
- A wall without an inner truss has a higher risk of buckling than a wall with an inner truss if the walls have the same shape and dimensions.

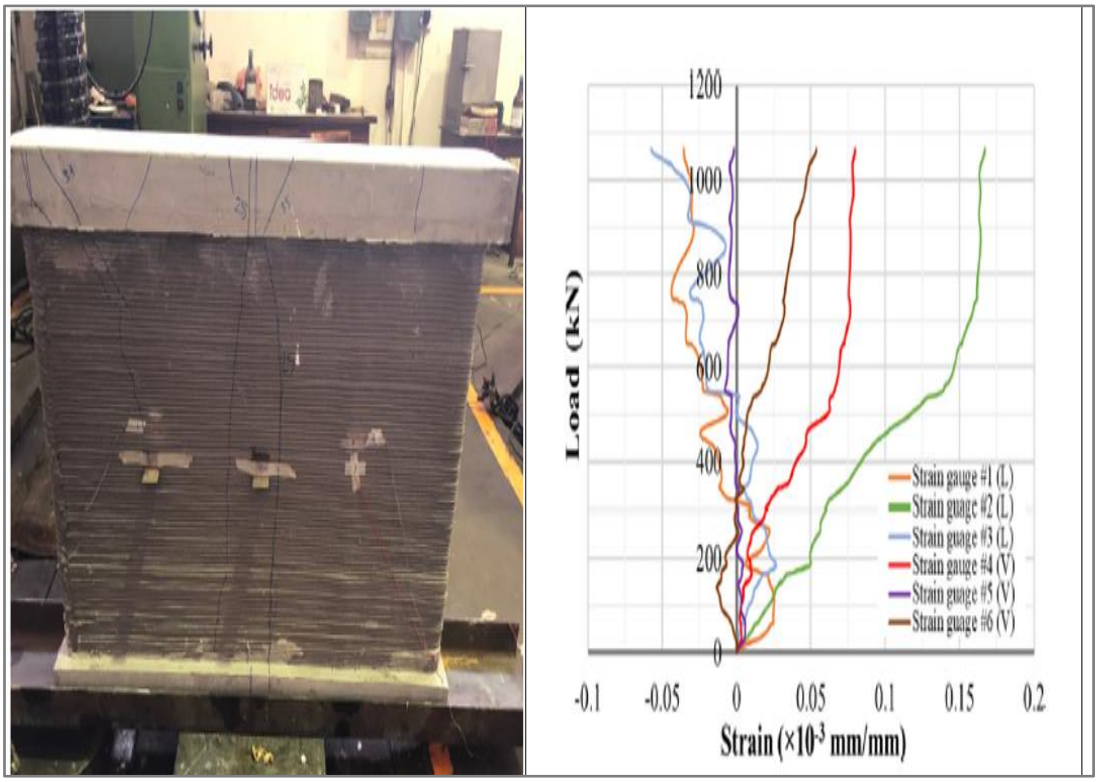

Figure 2.12 (Left) Cracking in the flat wall. & (Right) Strain of flat wall specimen (L = longitudinal direction, V = vertical direction) [27].

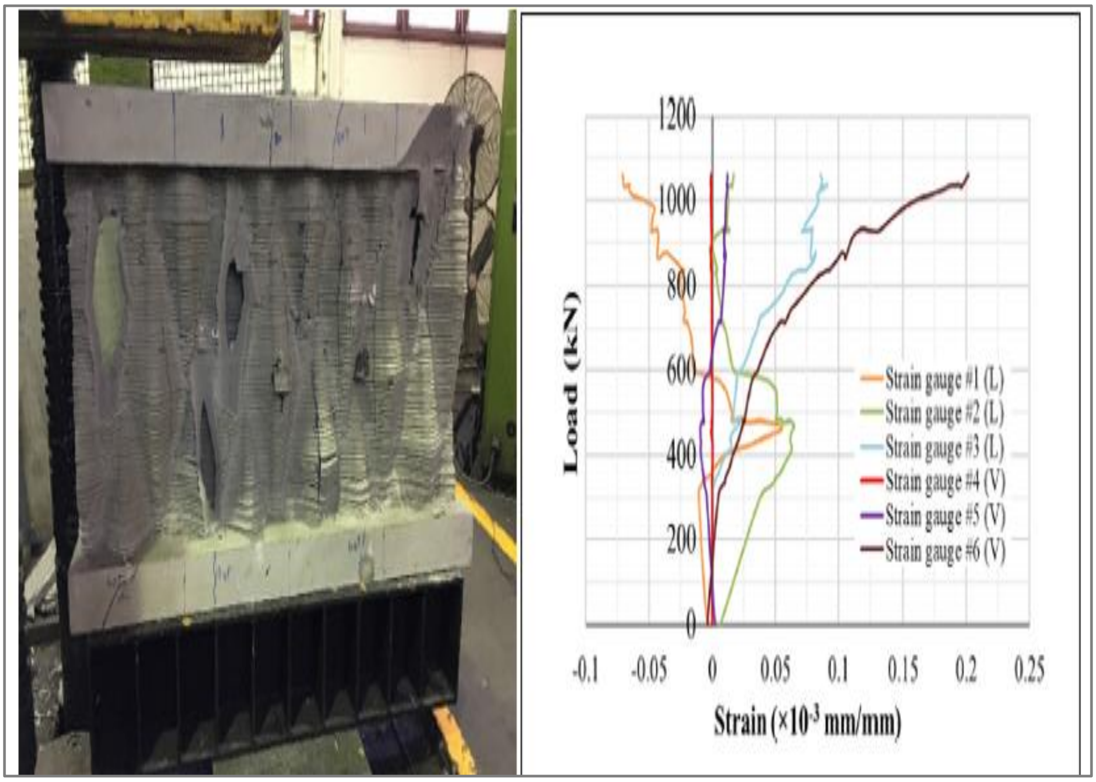

Figure 2.13 (Left) Diamond wall after the loading test. & (Right) Strain of the diamond wall specimen (L = longitudinal direction, V = vertical) [27].

(G. Tanapornraweekit et al., 2022) conducted the experimental and numerical investigation of 3D-printed mortar walls under uniform axial compression. The study investigates the behavior of 3D-printed plain and textured walls under uniform axial compression. The study aims to present the relevance of using 3D-printed mortar wall panels as load-bearing walls and proposes an analysis concept used with a finite element approach to investigate and capture the behavior of the 3D-printed walls. The study also examines how the shape and texture of the printed walls, as illustrated in Figure 2.14, influence the load transfer path, stress distribution, and geometrical non-linearity of the tested walls. The proposed finite element model is validated with the test results of the three tested walls. According to their research, the cross-section and texture pattern of the printed wall has an impact on the walls' stress distribution, load transfer path, and ductility. As can be observed from the higher overall performance of the diamond wall over the plain and carp walls, the symmetry of the printed pattern and the internal truss of the wall increases the specified mechanisms and qualities. Additionally, test results of both plain and textured walls were used to validate the proposed analytical idea for the 3D-printed wall construction [28].

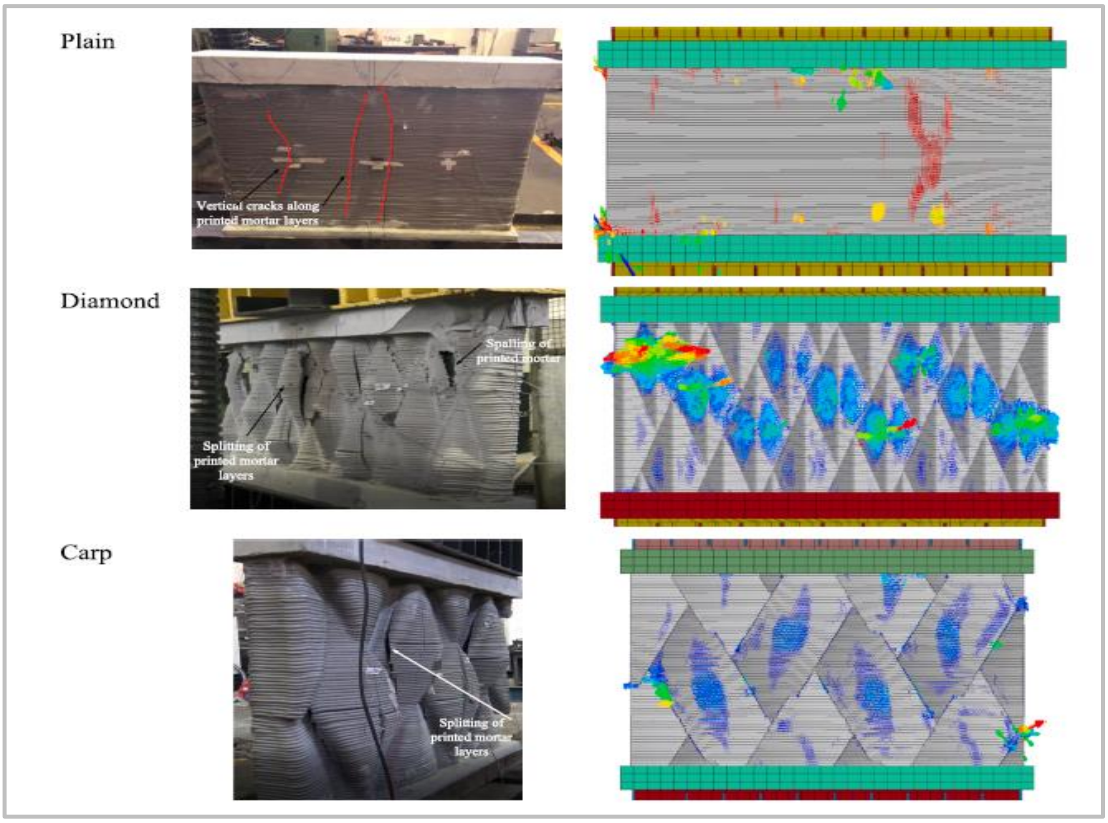

Figure 2.14 (a) and (b): failure mode of the walls without horizontal steel reinforcement; (c) and (d): failure mode of the walls with horizontal steel reinforcement [28].

(Xiaoyu Han et al., 2022) accomplished an experimental study on the structural mechanical properties and failure modes of large-scale 3D-printed concrete walls under axial compression loads. The study investigated the effects of horizontal steel reinforcement and the ratio of height to thickness on the behavior of eight 3D-printed concrete wall specimens. The results showed that the failure of 3D-printed concrete walls under axial compression is brittle and that the presence of horizontal steel reinforcement can improve their structural performance. The study provides valuable insights for informing the design and use of 3D printing technology in construction. Their study concluded that [4]:

- The axial compression strengths of 3D printed concrete at 28 days in two directions (one perpendicular to the cross-section of filaments and one perpendicular to the horizontal interfaces of layers) were 49.3 MPa and 40.8 MPa, respectively.
- The results revealed that 3D-printed concrete specimens exhibit a brittle failure mode under axial compression. The failure mode is characterized by vertical cracks that develop upward from the bottom, followed by the formation of vertical transverse cracks and the sudden collapse of the specimen. It should be noted that the cracking loads of the specimens were generally below 1250 KN. The ultimate bearing capacity could reach 3352.4 kN.
- Comparing the walls with different ratios of height to the thickness of 3, 5, 8, and 10, respectively, the ultimate bearing capacity first increased and then decreased.
- Horizontal steel reinforcement was found to reduce the ultimate bearing capacity of large-scale 3D-printed concrete walls under axial compression. The reduction coefficient due to the weakening effect of the horizontal steel reinforcement was 0.75. The layer where the horizontal steel reinforcement was set was the weak plane. The specimen with the horizontal steel reinforcement broke along the weak plane.

Figure 2.15 Failure mode of the walls without horizontal steel reinforcement; (c) and (d): failure mode of the walls with horizontal steel reinforcement [4].

In the synthesis of the literature review, the available studies have primarily centered on assessing the early age strength of printed walls and their concurrent behaviors during the printing process. Additionally, investigations have been directed toward comprehending the load-bearing capabilities with a keen emphasis on varying wall textures and the incorporation of horizontal reinforcement. Notably, a visible research gap has emerged concerning the comprehensive examination of the core component within the wall structure, a key aspect that significantly contributes to its stiffness and rigidity. Given the critical role this core component plays in the overall structural integrity, it is imperative to address this void through further examination. Thus, it is important for a subsequent study that thoroughly inspects this essential core element, exploring its influence and impact on the broader structural performance of 3D printed walls.

Chapter 3. Methodology

In this study, the main aim is to assess the load-bearing capacity and structural performance of 3D-printed concrete walls. Various wall-cross-section geometries have been selected for this study as shown in Figure 3.1.The most widely adopted additive manufacturing method for fabricating such walls which involves depositing mortar material layer by layer is the 3D printing of concrete using the parametric design capabilities of Grasshopper software (Figure 2.5) and ABB industrial robotic arm with 6-axis of freedom (Figure 3.2). Planning robotic paths, improving concrete printing procedures, and producing detailed designs for targeted printed walls are all possible uses for this integration. Additionally, rheological and mechanical properties were tested for prepared specimens of the same printed walls concrete mix to investigate the fresh and hardened properties of the used mix.

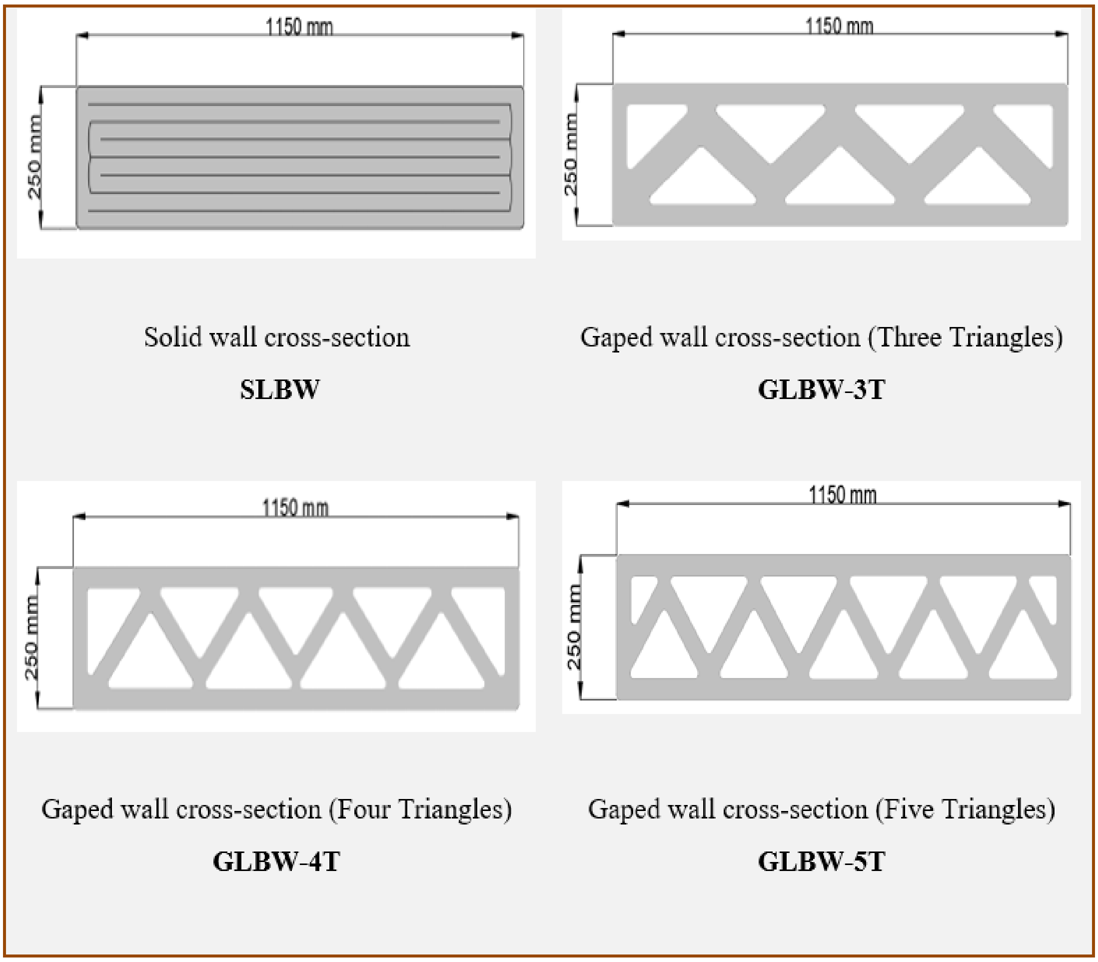

Figure 3.1 Walls cross-sections with different configurations.

Figure 3.2 3D ABB Robotic Arm by (Concretive Co.)

3.1 Materials

In this research, a premixed cementitious material supplied by Concretive Co. was utilized for printing the walls, ensuring the consistency and printing quality necessary for printing large-scale structural elements. Additionally, E6-glass fibers (GF), characterized by their properties detailed in Table 3.1, were incorporated to enhance the rheological and mechanical properties of the printed mortar. To achieve an optimal reinforcement effect, a dosage of 0.1% of the binder mass was carefully applied. While previous research by Pham et al. [29] emphasized the benefits of steel fibers in enhancing load-carrying capacity, this investigation focused on evaluating the impact of glass fibers (GF) on load-bearing performance, enriching the understanding of fiber reinforcement in 3D concrete printing applications.

Table 3-1 Physical properties of chopped E6-glass fibers.

Fibers Type	**Length (mm)**	**Filament Diameter (μm)**	**Specific Gravity (g/cm^3)**	**Tensile Strength (MPa)**	**Tensile Modulus (GPa)**
E6-Glass fibers	6 ± 1	13 ± 1	2.62 – 2.63	2500 – 2700	81

3.2 Fresh properties of 3DCP materials, (Rheological Testing Method)

Rheological testing of 3D concrete printing (3DCP) materials is a crucial aspect of ensuring the success and efficiency of the printing process. Rheology is the study of how materials flow and deform under applied forces, and it provides valuable information about the flow behavior, viscosity, and other important characteristics of fresh concrete during 3D printing. Here are some common rheological tests used for 3DCP materials that will be used in this study:

3.2.1 Flowability

Flowability refers to the ability of the concrete mixture to flow and pump smoothly through the 3D printer's nozzle and deposit layer by layer to create the desired structure. An optimal flowability ensures consistent extrusion, accurate placement, and adherence of the layers. Before casting test specimens for compressive strength testing, the slump (flow table) of concrete shall be measured and monitored for printing quality control purposes. The flow of proprietary 3D concrete mix shall be tested by ASTM C143 or ASTM C1611 [30, 31], whichever is applicable.

3.2.2 Extrudability

The 3DCP mixture should also be created for optimal extrudability, such that the extrudability of the concrete mixture is essential for achieving precise layering and maintaining the structural integrity of the printed object when passed through the delivery system and the printhead. Poor extrudability can lead to clogging of the nozzle, uneven deposition, filament bursting or split, and compromised print quality. To increase extrudability and reduce the risk of clogging in the printhead, cylindrical particles, and ingredients are frequently used [32].

3.2.3 Buildability

A key factor in assessing the performance of 3DCP mixtures for printability is buildability, which can be thought of as early-age stiffness. An extruded mix must be able to support its weight and the load of the succeeding layer while maintaining its cross-section with an acceptable level of deformation and without excessive settlement to have high buildability.

3.2.4 Setting time test

The setting time is a critical parameter in 3DCP, as it directly affects the buildability and overall construction speed. It refers to the time it takes for the fresh concrete to transition from a plastic, workable state to a solid state, where it gains sufficient strength to support its weight and the weight of subsequent layers during the printing process. In this study, the final setting time of the concrete mix was evaluated by Vicat Apparatus Test according to ASTM C191-04 [33].

3.3 Hardened Properties of 3DCP

The hardened properties of 3D concrete printing (3DCP) materials refer to the characteristics of the printed concrete structure after it has fully cured and attained its intended strength. These properties are critical in determining the structural integrity, durability, and overall performance of the 3D-printed object. Some of the key hardened properties of 3DCP materials include:

3.3.1 Compressive strength test

Compressive strength is one of the most crucial hardened properties of concrete. It represents the ability of the material to withstand axial loads and is determined by testing concrete cubes or cylinders. The compressive strength of 3DCP materials should meet the project's design requirements and applicable standards. In this investigation, both cast cubes with dimensions (50 x 50 x 50) mm and printed cubes with dimensions (70 x 70 x 70) mm were tested for compressive strength at 7 days as per ASTM C109 [34]. Moreover, the axial compression strengths of 3D printed concrete were carried out in three directions, one perpendicular (N) to the cross-section of filaments and one horizontal (P) to the interfaces of layers and the last one was longitudinal (L) to the printed filaments. Also, the average 7-day compressive strength shall be a minimum of 2500 psi (17.2 MPa) as per ICC/ AC509 [35] requirements for 3DCP load-bearing walls. The sample dimensions and load directions are illustrated in Figure 3.3.

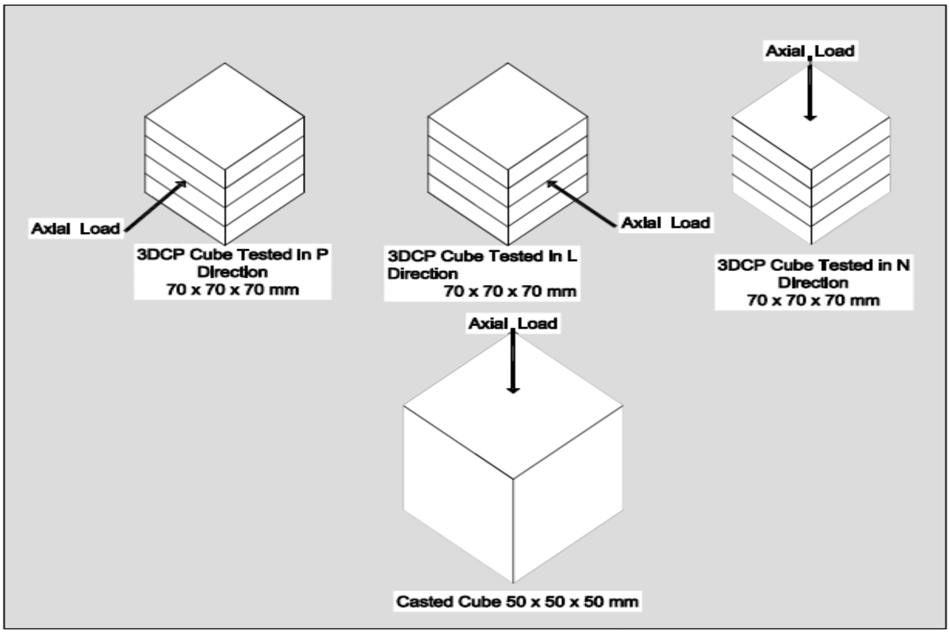

Figure 3.3 3DCP and cast cubes for compressive strength.

3.3.2 Flexural strength test

Flexural strength measures the ability of the concrete to resist bending or flexure. It is essential for structures subjected to bending forces, such as beams and slabs. The flexural strength of the 3DCP beam by applying a point load at the center line and the span length between the supports equals 3 times the depth as shown in Figure 3.4. Both printed and cast beams are to be flexural tested according to ASTM C78 standards [36]. Also, the printed beams will be investigated in both directions parallel (P) and perpendicular (N) to the filament directions as shown with dimensional details in Figure 3.5.

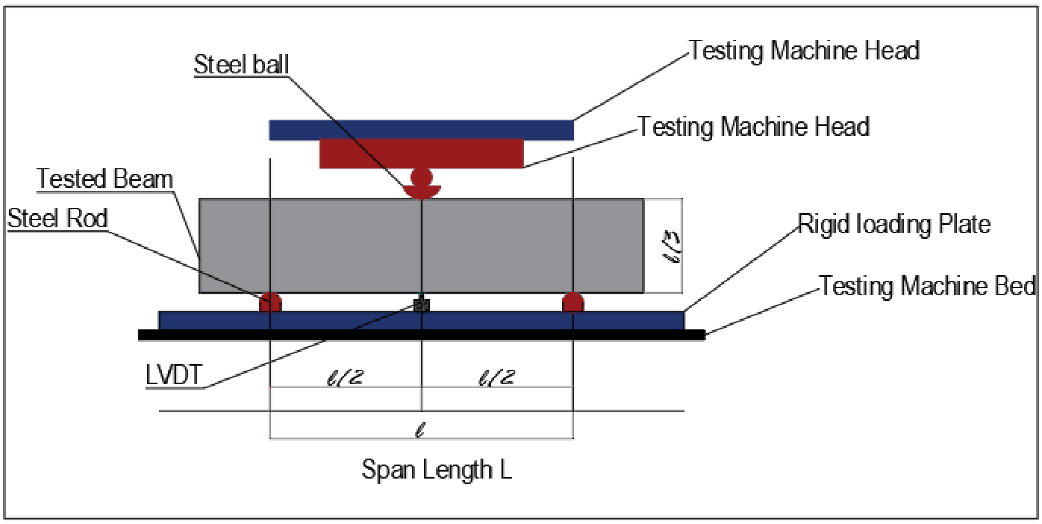

Figure 3.4 Schematic design of one-point loading flexural strength test.

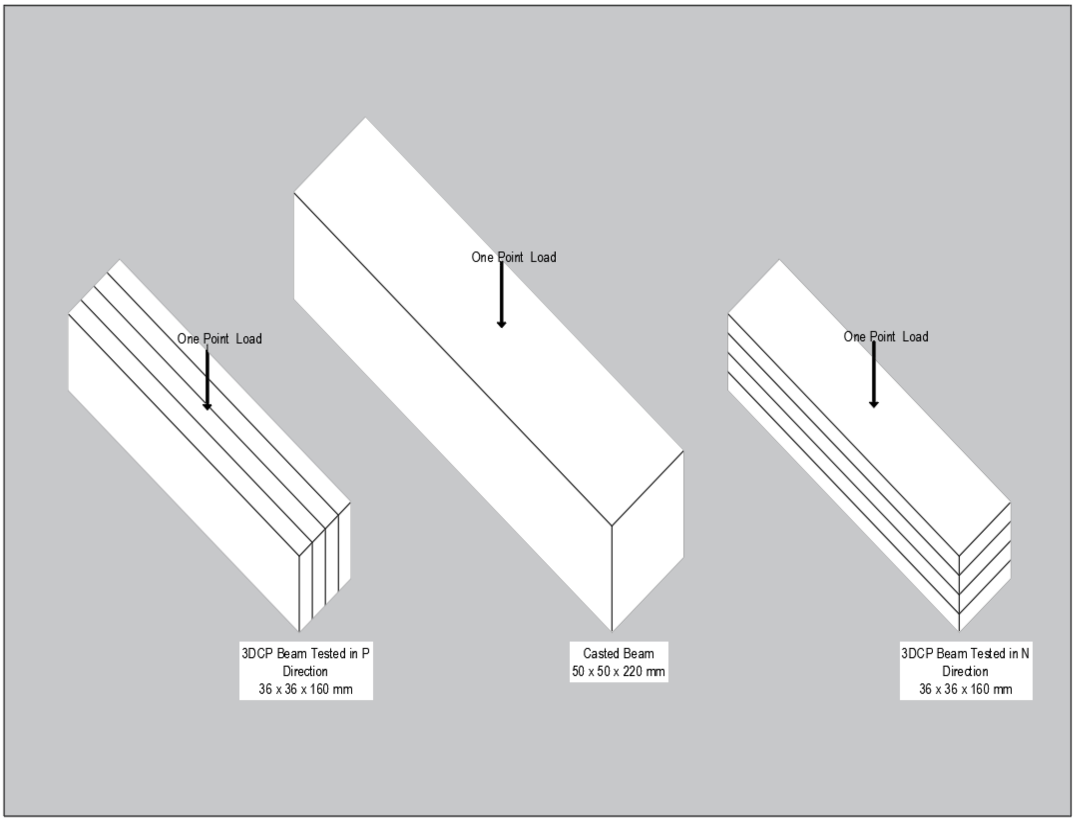

Figure 3.5 3DCP and Cast Beams for Flexural Strength.

3.4 3D Programing and Fabrication of Specimens

To start the process with geometry modeling of the printed walls, the model was formed using computer-aided design (CAD) software (Rhinoceros 3D version 6). Then, to slice the model, it has been transferred to the slicing software (Grasshopper). The thickness of each layer can be controlled as desired and the direction of the printing path of the extruding nozzle is also designed by the slicing software (Grasshopper). After the slicing process, the sliced model was transferred into the controller of the 3DP machine, and the printing operation began. A nozzle with a diameter of about 30 mm attached to the printhead will was used. The printed layer thickness is about 9 mm. Additionally, the printing process was closely monitored to ensure high-quality outcomes, focusing on factors such as consistent extruded material, smooth filament deposition, and precise alignment of printed layers. Furthermore, a steam vapor curing system was employed to maintain optimal temperatures and prevent heat-induced cracking, contributing to the overall quality and integrity of the printed walls.

3.5 Structural testing method

It has been presumed that the wall structure in this investigation was a load-bearing wall. Therefore, a compressive strength test was carried out to determine the wall structure's axial loading capacity. To evenly transfer the weight across the entire wall cross-section, a steel plate beam was simply supported the large-scale wall from the top. The reference direction and the wall dimensions are presented in Figure 3.6. Using a suitable test setup, a hydraulic mechanical testing machine was used to apply the load at the top of the wall specimen. A group of load cells, LVDTs, and strain gauges were installed at strategic locations on the wall to monitor the applied load, stress distribution, and deformations during the test. As shown in Figure 3.6, the wall specimens were placed into a uniaxial loading machine and loaded at a rate of 50 kN/min. During the testing, the strain, displacement, and map cracking in the wall were assessed. Further investigation of the structural performance and failure patterns was also evaluated.

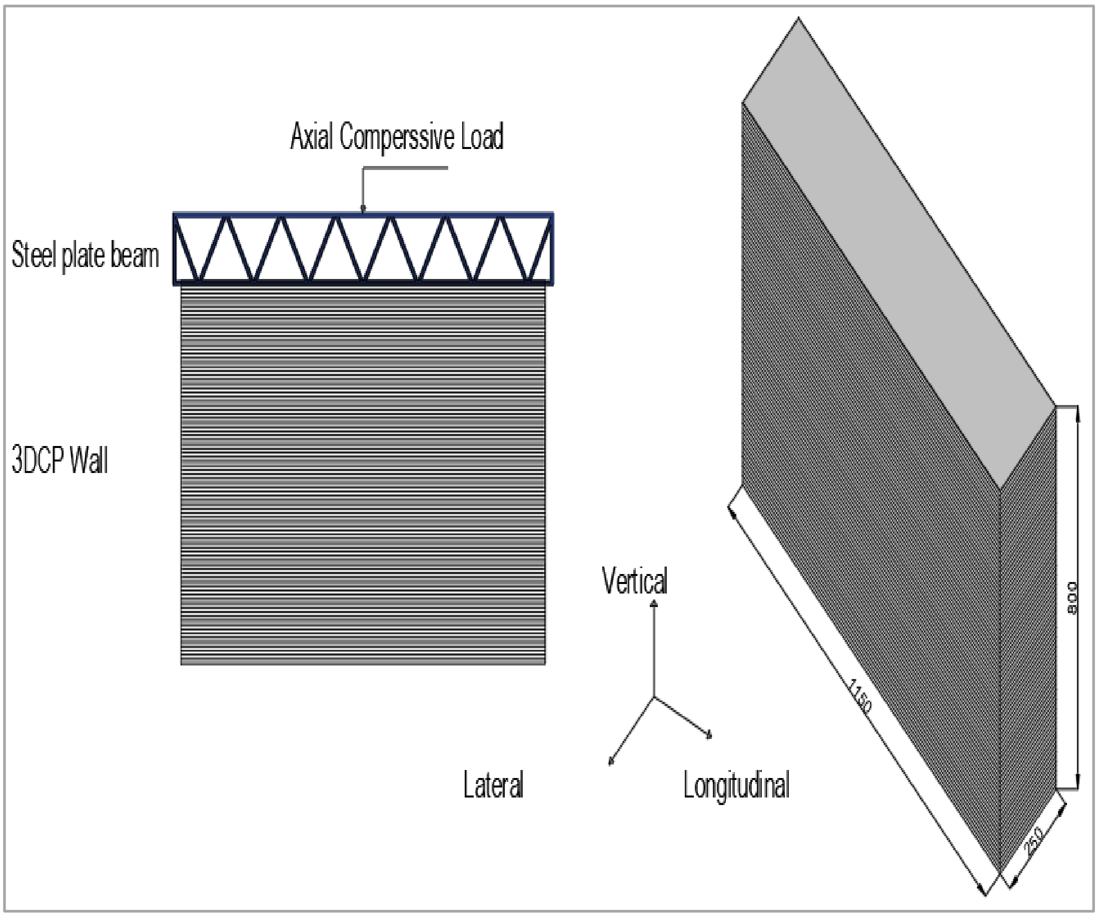

Figure 3.6 Schematic view of the tested wall and the setup, here dimnsions are in mm.

3.6 Experimental Program

In this study, a comprehensive investigation into the load-bearing capacity of 3D-printed walls has been conducted, encompassing a series of four distinct wall configurations. The cross-sectional layouts of these walls are visually depicted in Figure 3.1. It is important to highlight that the outer geometry of the wall is flat, as recommended by studies conducted by Daungwilailuk et al. (2021) [27] and Tanapornraweekit et al. (2022) [28]. These studies found that a waved texture contributes to higher tensile stress, leading to concrete spalling and cracking on the wall face. Therefore, the experimental focus shifts towards large-scale 3D printed flat walls featuring a W-type infill as a pracing system, accurately crafted to facilitate axial compression loading tests. A prominent aspect of these walls is the integration of the core truss within their design, strategically intended to evaluate the structural rigidity and effectively counteract deformation under varying loads. As shown in Figure 3.6 all specimens share uniform dimensions, owing a thickness of 250 mm, a height of 800 mm, and a length of 1150 mm. Central to the objectives of this study is the thoughtful manipulation of the cross-sectional configuration, wherein an intended purpose is to modify the number of truss members. This involves a progressive alteration in the number of triangle-shaped members, ascending from three to four to five. Such manipulation is carried out to distinguish the direct influence of truss complexity on load-bearing behavior.

The axial compression testing procedure, fundamental to the study's objectives, is precisely designed and arranged. These tests were performed within the controlled environment of the laboratory, employing standard load increment protocols. Loading was systematically applied in a load control manner with rate of 50 KN/Min. The axial load was distributed uniformly by the placement of a steel beam atop the respective walls. In order to capture and analyze crucial data during the axial compression tests, an array of appropriate instrumentation has been utilized. Linear variable displacement transformers (LVDTs) are positioned to record both vertical and horizontal displacements, affording precise insights into structural behavior. Simultaneously, strain gauges were used to monitor concrete strains, giving vital information regarding material response.

All walls are printed with consistent parameters which are presented in Table 3.2. These primary 3D printing parameters include a printed layer thickNess of 90 mm, layer width ranging from 35 to 36 mm, printing speed between 90 and 100 mm/min, nozzle size of 30 mm, and air curing temperature maintained at 27°C.

Table 3-2 3D printing parameters.

Parameters	Evaluation Remark
Printed layer thickNess (mm)	9
Width of each printed layer (mm)	35
Printing speed (mm/min.)	90-100
Size of printing nozzle (mm)	30
Air curing temperature (^{0}C)	27

Likewise, an assessment of the fresh properties of the utilized mix was conducted, employing the testing methods outlined in the preceding section. The relevant fresh properties examined in this investigation are outlined in Table 3.3, with detailed results and discussions provided in Chapter 4.

Table 3-3 Fresh properties testing of 3DCP materials.

Evaluation of the fresh properties parameters
Bulk Density of the 3D extrusion mortar (kg/m^3)
Flow table test (at 25 drops) (mm)
Final setting time (mins)
Air content of the fresh mortar (%)

In terms of mechanical testing, samples were extracted from the same mix utilized in wall construction, as detailed previously. These mechanical assessments are crucial for evaluating the hardened strength of the concrete. Three primary mechanical tests were performed, involving: compressive, flexural, and tensile evaluations. To understand the material's behavior of the 3DPC, tests were conducted in multiple directions to ascertain orthotropic behavior as a composite perspective. Table 3.4 provides a summary and specifics of the tested samples, including both cast and printed cubes for compressive strength, cast and printed prisms for flexural testing, and cast dog bone samples for tensile assessment. Each test comprised three samples, with the average value determined in accordance with ASTM testing standards. Detailed results and discussions can be found in the forthcoming chapter.

Table 3-4 Mechanical Performance Testing.

Test Name	Sample Designation	Sample's Size mm	Number of samples
Compressive strength (MPa)	Cast Cube	50 x 50 x 50	3
	Printed Cube (N) *	70 x 70 x 70	3
	Printed Cube (P) *	70 x 70 x 70	3
	Printed Cube (L) *	70 * 70 * 70	3
Flexural Strength (MPa)	Cast Prism	220 x 50 x 50	3
	Printed Prism (N)	160 x 36 x 36	3
	Printed Prism (P)	160 x 36 x 36	3
Tensile Strength (MPa)	Cast Dog bone Samples	330 x 60 x 30	3

(N) Normal, (P) Parallel, and (L)* Longitudinal to the printed filaments.*

Referring to Table 3.5, which presents valuable information regarding the comprehensive structural performance assessment and evaluation conducted in this study. Each wall undergoes assessment based on several key parameters: the printed area and total volume, load-bearing capacity including loading characteristics such as the initiation of the first crack and the maximum testing load just before collapse, and deformation characteristics measured by the maximum vertical and lateral displacement using LVDTs. Strain gauges were strategically placed to monitor wall strain during load-bearing tests, capturing both tensile and compressive stress. Additionally, the cracking behavior and pattern were analyzed to determine maximum crack width, crack maps, crack intensity, and overall wall rigidity.

To sum up, this study manipulates cross-sectional configurations to examine the impact of truss complexity on load-bearing behavior. Through this research, a deeper understanding of the load-bearing capacity of 3D-printed walls is gained, contributing to the advancement of construction practices and engineering knowledge. Moreover, the optimal solution will be determined by identifying the most satisfactory wall behavior, which can then serve as the basis for conducting an in-depth factorial study in the future.

Table 3-5 Structural load bearing capacity testing and structural evaluation.

Specimen / Evaluation	GLBW-3T	GLBW-4T	GLBW-5T	SLBW
Cross-section Configuration	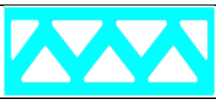		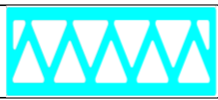	
Wall Size (mm)	1150 x 800 x 250	1150 x 800 x 250	1150 x 800 x 250	1150 x 800 x 250
Cross-section Description	The core zone is formed by 3 triangles, which collectively constitute 6 truss members.	The core zone is formed by 4 triangles, which collectively constitute 8 truss members.	The core zone is formed by 5 triangles, which collectively constitute 10 truss members.	The core zone is fully solid of printed adjacent layers.
Cross-sectional Area m^2	The total cross-sectional area was calculated as per the printed layout of each wall considering the printed segments.			
Area Percentage %	Calculating the percentage of the printed wall's cross-sectional area relative to the total area.			
Wall Volume m^3	The total volume of the extruded materials of each wall.			
Wall Printing Time (min)	Assessing the total time taken for the complete printing of each wall.			
Cracking Load (kN)	During the structural testing, the first crack is essential to be determined.			
Max-Load (kN)	Based on the last recorded load when the test is terminated.			
Max-Crack Width (mm)	The observed max-crack width was measured by a digital concrete crack width meter.			
Max Buckling (mm)	Maximum recorded lateral displacement of the wall carried out by horizontal LVDT.			
Max-V-Displacement (mm)	Maximum recorded vertical displacement of the wall carried out by vertical LVDT.			
Max tensile strain (mm/mm)	The maximum tensile strain recorded by the horizontal strain gauges on the wall.			
Max compressive strain (mm/mm)	The maximum compressive strain recorded by the vertical strain gauges on the wall.			
Cracking Intensity and pattern	Assessing the crack intensity and the pattern of the crack maps (horizontally, vertically and transversely) of each wall.			
Element Rigidity after Testing	Evaluation of the wall rigidity of the wall after the termination of the test.			

Chapter 4. Results and Discussions

This chapter presents a series of experiments focusing on fresh and hardened properties of the concrete mix, as well as the structural performance of 3D Concrete Printing (3DCP) walls. The investigation includes assessing load-bearing capacity and structural behavior through four distinct wall configurations as shown in Figure 3.1. These large-scale walls feature a W-type infill and integrate a core truss design to enhance structural rigidity. All specimens share uniform dimensions and undergo axial compression testing in a controlled laboratory environment with a load rate of 50 kN/min. Tests are conducted using standard load increment procedures, with instrumentation such as LVDTs and strain gauges to capture data on displacements and concrete strains. The walls are printed with consistent parameters detailed in Table 3.2. Overall, this chapter provides comprehensive experimental and analytical assessments of fresh, hardened, and structural properties.

4.1 Fresh properties testing (Rheological testing)

In this study, premix cementitious materials supplied by Concretive Co. have been utilized in this research. Glass fibers (GF) with dimensions of 13 μm in diameter and 6 mm in length were incorporated into the mix at a dosage of 0.1% relative to the total mass to enhance interface bonding between printed layers. The rheological properties of the used mix were evaluated to ensure consistency, workability, extrudability, and buildability, thereby preventing cracking and segregation on the concrete-printed surface. The addition of glass fibers (GF) aimed to further improve these rheological properties. Table 4.2 presents detailed information regarding the workability, setting time, and other relevant rheological properties of the extrusion material.

Table 4-1 Fresh properties testing of 3DCP materials.

Parameters	**Evaluation Remark**
Bulk density of the 3D extrusion mortar (kg/m^3)	2300
Flow table test (at 25 drops) (mm)	210
Final setting time (mins)	85
Air content of the fresh mortar (%)	2.6

4.2 Hardened properties testing (Mechanical testing)

The mechanical properties of the used concrete mix were evaluated through experimental investigations, particularly focusing on compressive, flexural, and tensile strength characteristics. Samples were categorized as cast and printed, with different testing methodologies applied to each category. The testing direction concerning the printing direction is illustrated in Figure 4.1 for clarity. Details of the test results are summarized in Table 4.2.

Table 4-2 Mechanical Performance Testing.

Test Name	Sample Designation	Sample's Size (mm)	Number of samples	Average
Compressive strength (MPa)	Cast Cube	50 x 50 x 50	3	85
	Printed Cube (N) *	70 x 70 x 70	3	58
	Printed Cube (L) *	70 x 70 x 70	3	48
	Printed Cube (P) *	70 x 70 x 70	3	40
Flexural Strength (MPa)	Cast Prism	220 x 50 x 50	3	12.3
	Printed Prism (N)	160 x 36 x 36	3	11.8
	Printed Prism (P)	160 x 36 x 36	2	10.4
Tensile Strength (MPa)	Cast Dog bone	330 x 60 x 30	3	6.2

Note: (N) Normal to the printed filament, (L) Longitudinal to the printed filament. (P) Parallel to the printed filament.*

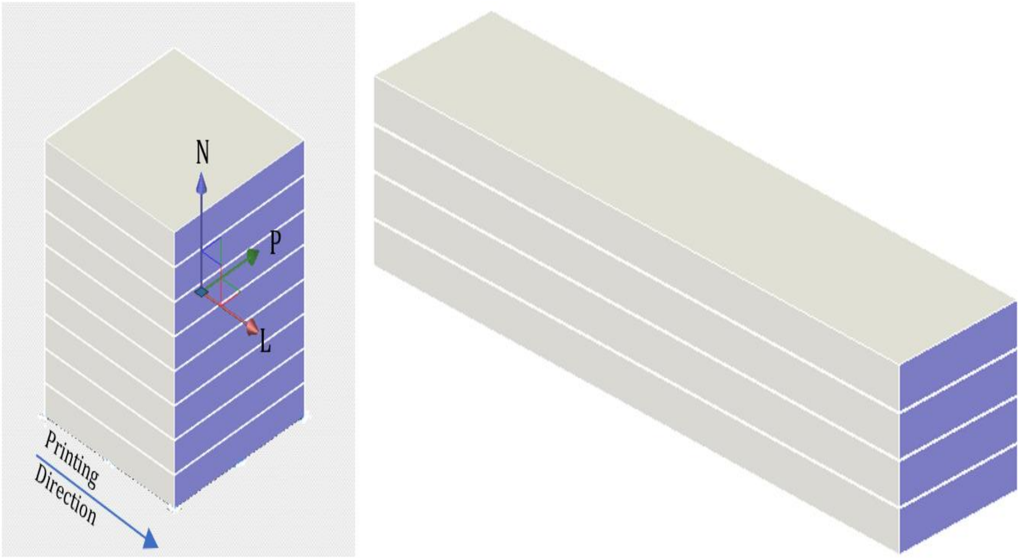

Figure 4.1 Testing direction concerning the printed filaments

4.2.1 Compressive strength test results

For compressive strength assessment, three cast concrete cube specimens (50 x 50 x 50 mm) were tested, yielding an average strength of 85 MPa. The test results and tested samples are shown in Figure 4.2-a. In contrast, nine printed concrete cubes (70 x 70 x 70 mm) shown in Figure 4.2-(b, c & d) were tested in three directions, denoted as N, L, and P, corresponding to perpendicular, longitudinal, and parallel orientations to the filaments' cross-sections as illustrated in Figure 4.1. Results exposed varying strengths in these directions, with values of 58 MPa, 48 MPa, and 40 MPa, respectively for each direction. The compressive strength of 3DCP in the N direction reached 68% of the cast strength, while in the L and P directions, it achieved 56% and 47%, respectively. Notably, the direction of extrusion led to density variations in the printed layers, with the N direction exhibiting significantly higher density due to the closer packing of material caused by high pumping pressure during extrusion. Additionally, the bond strength between two adjacent printed layers, as observed in the L and P directions, contributed to minimizing the overall strength, as depicted in the failure phase in Figure 4.2. These factors collectively indicate that 3DCP behaves as an orthotropic material due to differing contact areas of the extruded beads [37].

(a) Compressive Testing For The Cast Cubes.

81.7 MPa | 85 MPa | 88.2 MPa

(b) Compressive Testing For The Printed Cubes Normal To The Printed Filaments.

67 MPa | 46 MPa | 60 MPa

(c) Compressive Testing For The Printed Cubes Parallel To The Printed Filaments.

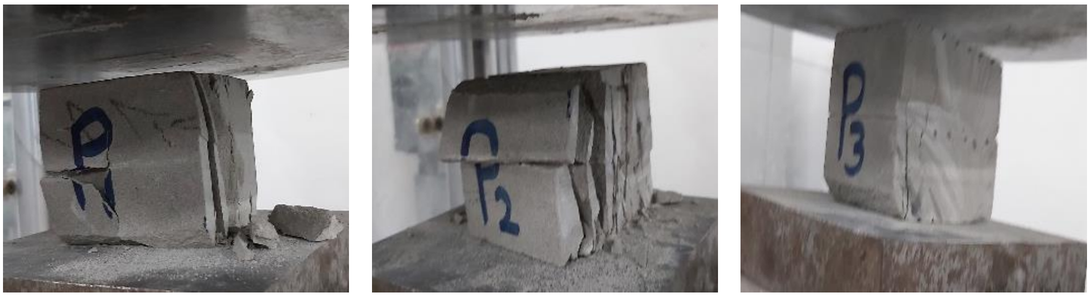

39 MPa | 40 MPa | 40 MPa

(d) Compressive Testing For The Printed Cubes Longitudinal The Printed Filaments.

46 MPa | 45 MPa | 54 MPa

Figure 4.2 Compressive Tests for Cast and Printed Samples

4.2.2 Flexural strength test results

Furthermore, flexural tests were conducted on three cast concrete prisms with dimensions of 220 x 50 x 50 mm, yielding an average strength of 12.3 MPa (Figure 4.3 - a). Similarly, five printed prisms measuring 160 x 36 x 36 mm were tested in both N and P directions, resulting in average strengths of 11.8 MPa and 10.4 MPa, respectively, as depicted in Figure 4.3 - (b & c). The results indicate that the printed flexural strength was 96% in the N direction and 85% in the P direction, suggesting that printing has less influence on strength due to the line-based load application, which minimizes the impact of shape and the contact areas of the printed layers compared to the compressive test.

(a) Flexural Tests for Cast Prisms

9.85 MPa | 10.3 MPa | 16.7 MPa

(b) Flexural Tests for Printed Prisms Perpendicular to The Printed Filaments.

9.4 MPa | 13.87 MPa | 12.3 MPa

(c) Flexural Tests for Printed Prisms Parallel to The Printed Filaments.

13.3 MPa | 7.6 MPa

Figure 4.3 Flexural Tests for Cast and Printed Prisms

4.2.3 Tensile strength test results

The evaluation of tensile strength involved testing cast dog-bone samples prepared and assessed according to ASTM D638-14 standards [38], yielding an average strength of 6.2 MPa, as depicted in Figure 4.4. This average value reflects the material's ability to withstand tensile stresses before failure. Furthermore, analyzing the fracture surfaces of the dog-bone samples post-testing provides insights into the material's failure mechanisms and fracture behavior, suggesting a brittle failure mode.

Tensile Strength Test For Dog Bone Samples	
	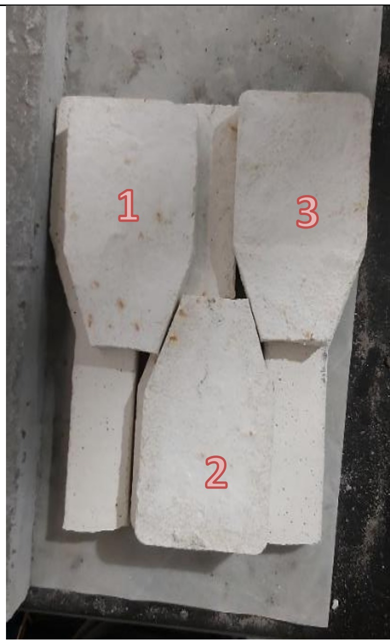
(5.8, 6.3, 6.4) MPa for samples# 1, 2, and 3 respectively.	

Figure 4.4 Dog Bone Tensile Test

In summary, the study investigated the mechanical properties of a concrete mix through compressive, flexural, and tensile strength tests. Results listed in Table 4.2 showed varying strengths in printed samples compared to cast ones, highlighting the influence of printing direction on density and strength distribution. Flexural tests revealed minimal printing effects on strength. Tensile tests indicated the material's ability to withstand stress before failure, with a brittle failure mode observed. These findings enhance the understanding of 3DCP's mechanical behavior of the used mix and its implications for structural performance of the 3DCP elements including 3DCP load-bearing walls studied in this case.

4.3 Examination of Structural Performance of 3DCP Walls and Outcome Analysis

Building upon the earlier discussion in Chapter 3 concerning the selected walls for testing, a total of four walls with different configurations, identified as LBWs, underwent advanced testing and evaluation. Figure 4.5 illustrates the Instron Universal Machine and the test setup. To ensure uniform distribution of the applied axial loading, a steel beam was positioned at the top of each wall specimen. The test progress was monitored through an operation control, with data being recorded at a frequency of 10 times per second. The loading was applied in a monotonically increasing manner in a single step, with a loading rate of 50 KN/m. For the measurement of vertical and horizontal displacements, Linear Variable Displacement Transformers (LVDTs) were employed, while strains in the concrete were recorded using strain gauges. Figure 4.6 - (a & b) provides one of the tested walls with the representation of the positions of these strain gauges and LVDTs on the specimens.

Figure 4.5 Instron Compression machine and test setup view.

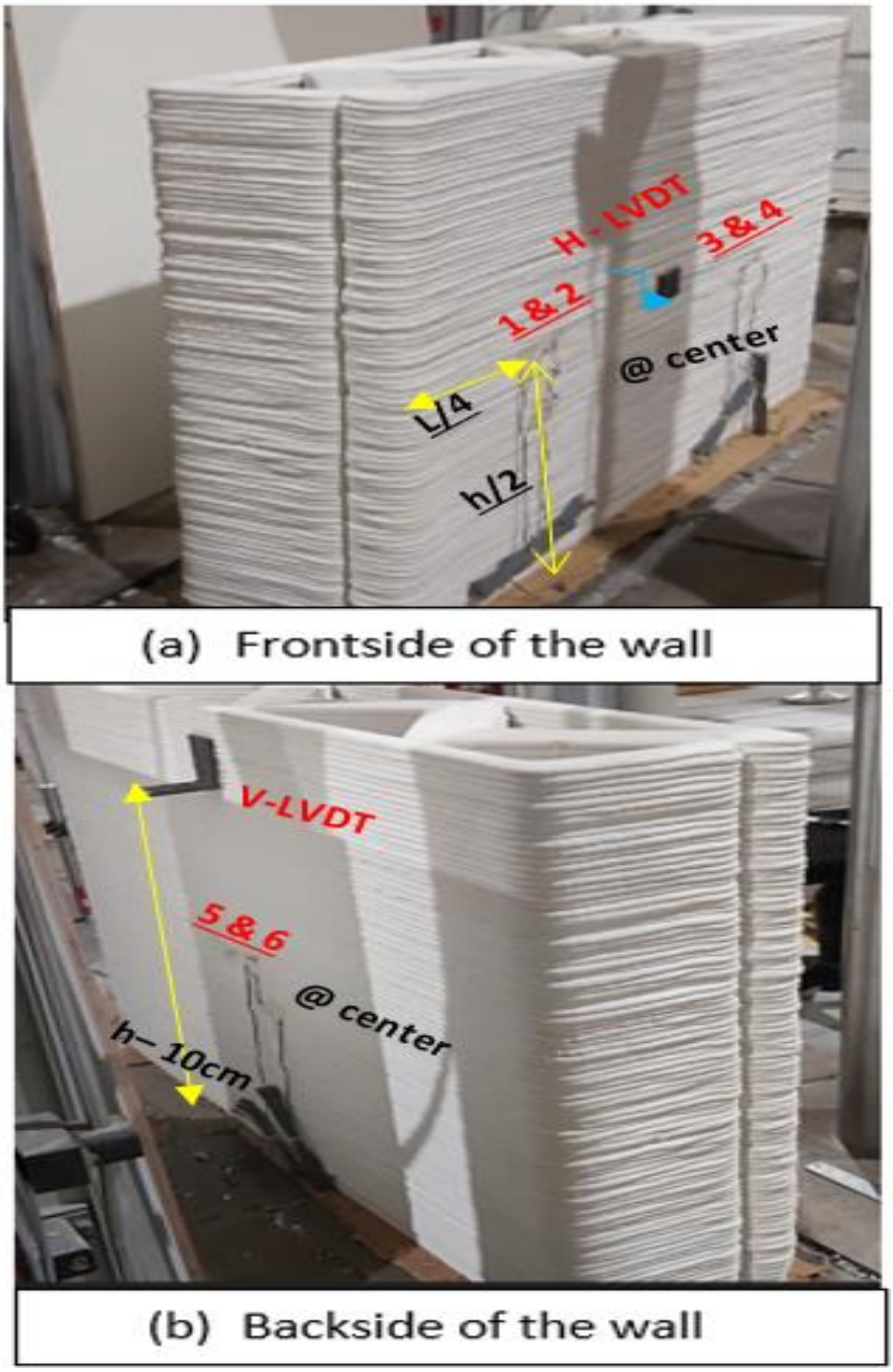

Figure 4.6 Positions of strain gauges and LVDTs.

This assessment primarily focused on determining the maximum load-bearing capacity, and deformation and analyzing the failure behavior of each wall. Each wall underwent a comprehensive analysis, during which its behavior was carefully observed and documented, particularly in terms of crack patterns and deformations occurring as load increments were applied. The specific outcomes of the tests for each wall are detailed in the subsequent subsections.

4.3.1 GLBW-3T load-bearing wall testing

Figure 4.7 GLBW-3T Dimensions and Configuration

Figure 4.7 represents GLBW-3T wall showing the 3D drawing details and cross-section. The core zone of the wall consists of double layers that form three triangles acting as a truss. A compressive load was applied on the top of this wall to determine its load-bearing capacity. The experimental findings have been presented through various measurements and observations. Load-displacement relationship for the tested wall has been graphically shown in Figure 4.8-a, providing a visual representation of the wall's response to the applied loads. Accordingly, the maximum vertical displacement recorded by the testing machine was 5.15 mm for the maximum load of 1516 kN. In addition to that, the deformation measurements by LVDTs were conducted along both X and Z axes as shown in Figure 4.8-b, and the recorded vertical displacement was about 1.69 mm under a load of 1500 kN, while the maximum lateral displacement reached 1.48 mm at 1510 kN. Figure 4.8-c illustrates the results distribution of strain gauges in both horizontal (tension zone) and vertical (compression zone) orientations. In the horizontal direction, strain gauge #1 reveals a distinctive shift from tensile to compressive strain at 350 kN preceding the first observed crack at 450 kN. Maximum tension strain is recorded by strain gauge #3 at 1509 kN, reaching 281 µmm/mm In the compression zone, strain gauges #2, #4, and #6 record maximum strains of 173 µmm/mm at 320 kN, 104 µmm/mm at 505 kN, and 140 µmm/mm at 350 kN, respectively. The strain gauge data shows steady increases in both tension and compression zones at the entail loading before the first crack, followed by fluctuations during crack development.

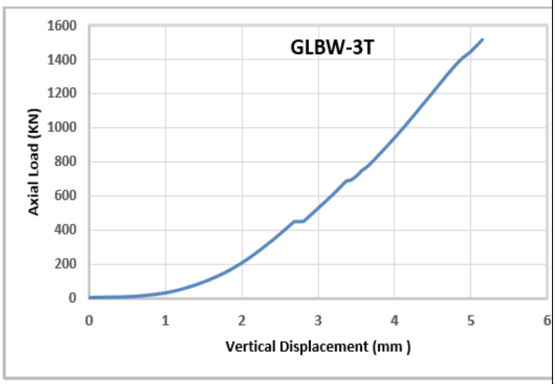

(a) Load-displacement relationship

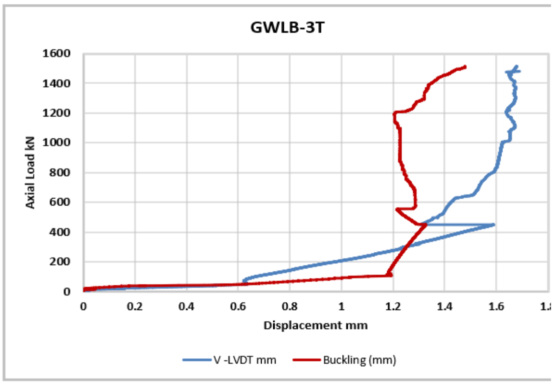

(b) Load vs deflection and buckling.

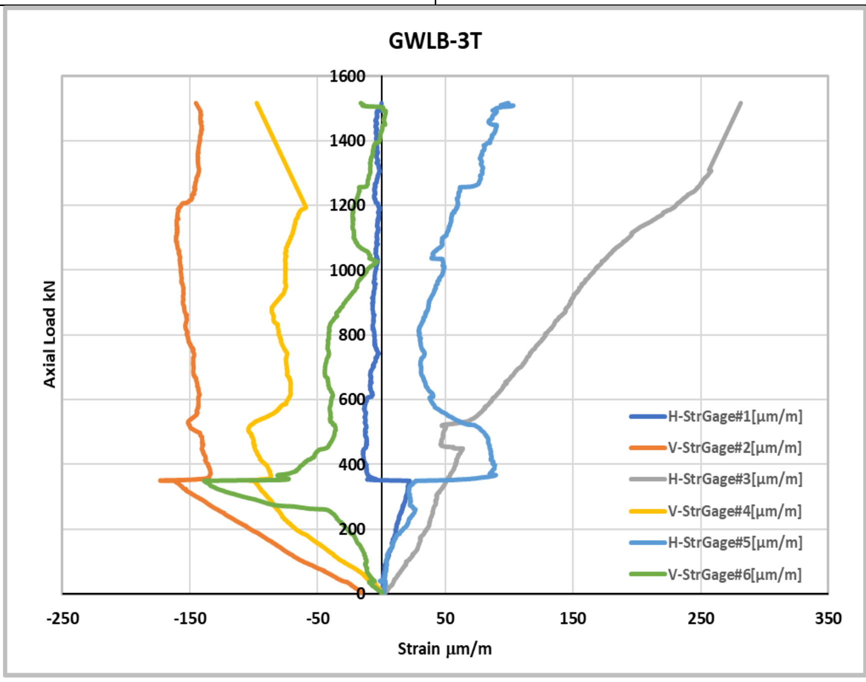

(c) Vertical and Horizontal strain gauges results.

Figure 4.8 GLBW-3T Testing Results

The GLBW-3T wall specimen exhibited an initial crack at approximately 450 kN (Figure 4.9-a), followed by vertical propagation from top to bottom. Throughout the test, the structural integrity of the wall remained intact, without bulging, spalling, or visible horizontal cracks at the printed layer interfaces. The most significant crack width observed was 3.6 mm at a load of 1450 kN. Demonstrating remarkable load-bearing capacity, the wall sustained a maximum load of 1516 kN However, the test was halted due to safety concerns, indicating its potential to withstand even higher loads. Vertical cracks along the wall's sides initiated at 625 kN and propagated downward to 1475 kN, revealing insights into its structural behavior under loading increments (Figure 4.9-b). Figure 4.9-c depicts cracks on the top of the wall and the behavior of its core zone following the conclusion of the test.

(a) First crack @ 450 KN

(b) Vertical and transfer cracks along the wall's sides

(c) GLBW-3T cross-section after testing.

Figure 4.9 GLBW-3T Cracks and Failure Patterns

While GLBW-3T was initially designed with two adjacent printed layers, the configuration posed challenges when transitioning to ascending walls. Specifically, the increased number of truss members in walls GLBW-4T and GLBW-5T resulted in sharp angles, complicating the printing path programming and causing overlap between layers at these angles. Furthermore, these sharp angles adversely affected the stability of the wall face, particularly at the contact area between the wall's face and the tips of the core zone part, leading to plastic failure during the printing process, as illustrated in Figure 4.10. Consequently, the research scope was adjusted to print a single layer instead of two adjacent layers, as in the GLBW-3T case. This modification will decrease the volume of printed concrete and the corresponding cross-sectional area. As a result, there will be a slight impact on the bearing capacity and structural performance of the walls.

Figure 4.10 Sharp angles effect on the printing stability.

4.3.2 GLBW-4T Load Bearing Wall Testing

The second tested wall, identified as GLBW-4T and described in Figure 4.11, shares the same monolithic dimensions as the other walls, with a core zone comprising 4 triangles and 8 truss members. The findings from the wall testing are as follows: Firstly, load-displacement relationships were graphically presented in Figure 4.12-a, indicating a maximum vertical displacement of 5.8 mm recorded by the machine, corresponding to a load bearing of 1704 kN.

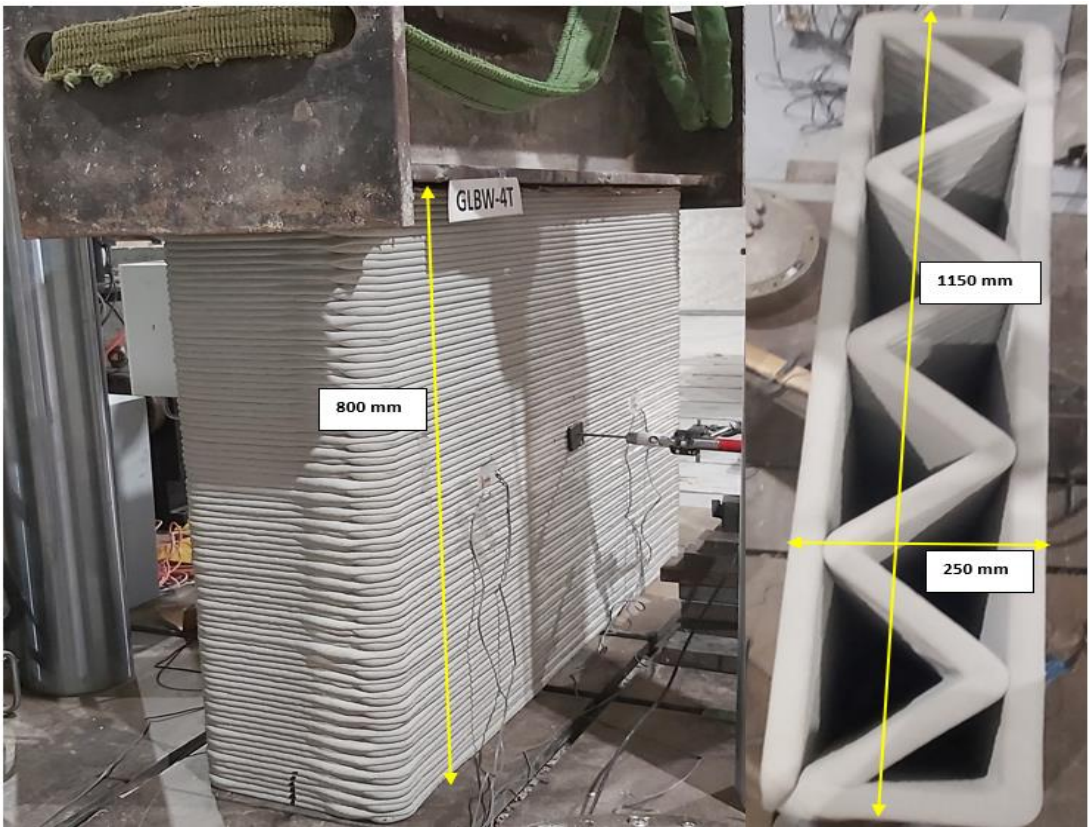

Figure 4.11 GLBW-4T Dimensions and Configuration

The maximum recorded vertical displacement was 1.72 mm under a load of 1442 kN, with a maximum lateral displacement of 1.77 mm at 1500 kN as presented in Figure 4.12-b, after which the LVDTs were removed due to safety concerns. Additionally, strain gauges were installed to record strain in both the vertical and horizontal directions on both the front and back faces of the walls, as shown in Figure 4.11-c. The readings fluctuated due to the sensitivity of strain gauges and sudden movements during cracking. The maximum compression strain recorded by strain-gauge#6 was 161 μm/mm and the maximum tension strain recorded by strain-gauge#1 was 64 μm/mm, corresponding to loads of 548 kN and 735 kN, respectively.

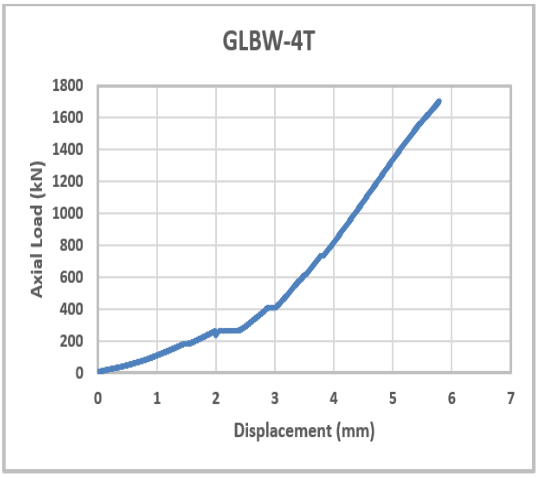

(a) Load-displacement relationship

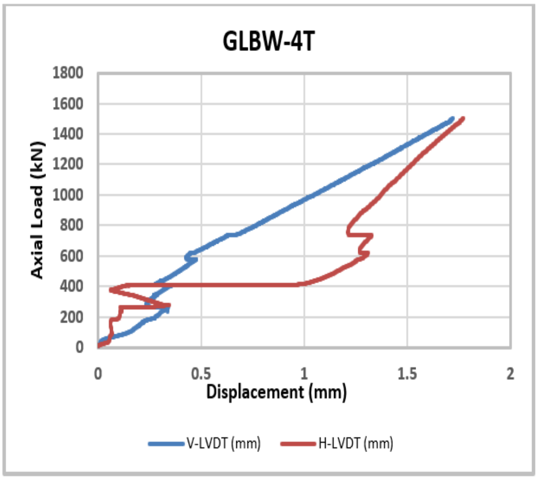

(b) Load vs deflection and buckling.

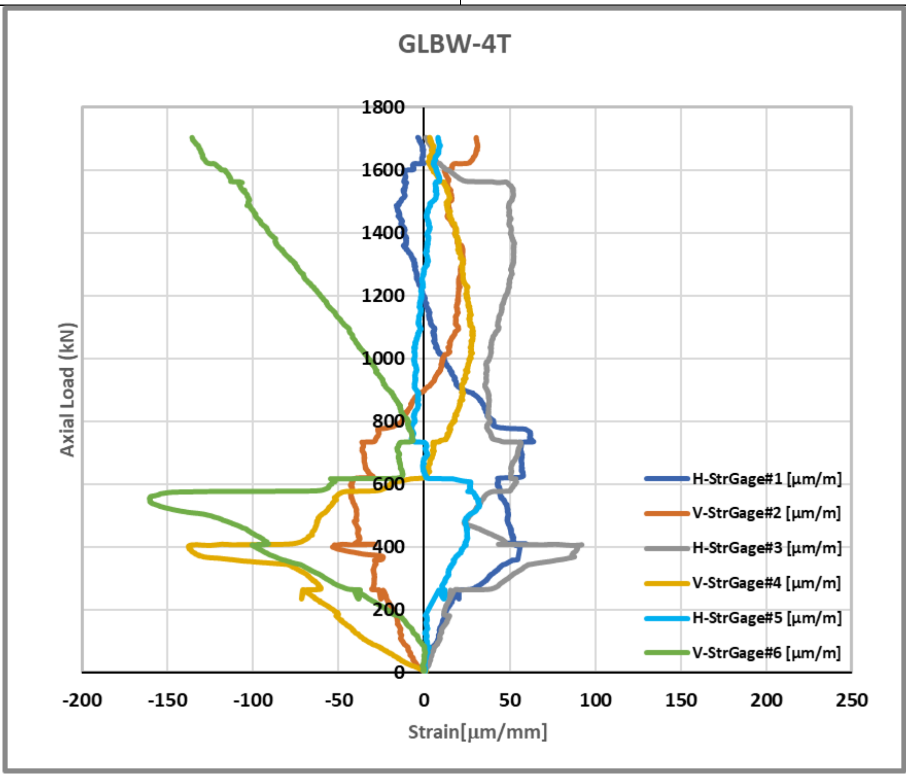

(c) Vertical and Horizontal strain gauges results.

Figure 4.12 GLBW-4T Testing Results

Notably, the most substantial crack width observed was 9.6 mm at a load of 1630 kN. The wall specimen exhibited a maximum load capacity of 1704 kN, leading to the test's termination due to safety concerns, signifying its ability to withstand loads exceeding this value. For the GLBW-4T specimen, the first crack appeared at approximately 295 kN shown in Figure 4.13-a, followed by vertical propagation from top to bottom on the front side of the wall. Subsequently, cracks were observed on the left side vertically at loads of 490 kN and transversely on the front side at 500 kN presented in Figure 4.13-

b. It is important to note that spalling and splitting of the left corner part were observed at the end of the test after the removal of the top steel beam 4.13-c. As shown in the figure, no visible horizontal cracks were observed at the interface between the printed layers during the test, except for the split part.

(a) First crack @ 295 KN

(b) Vertical and transfer cracks along the wall's sides

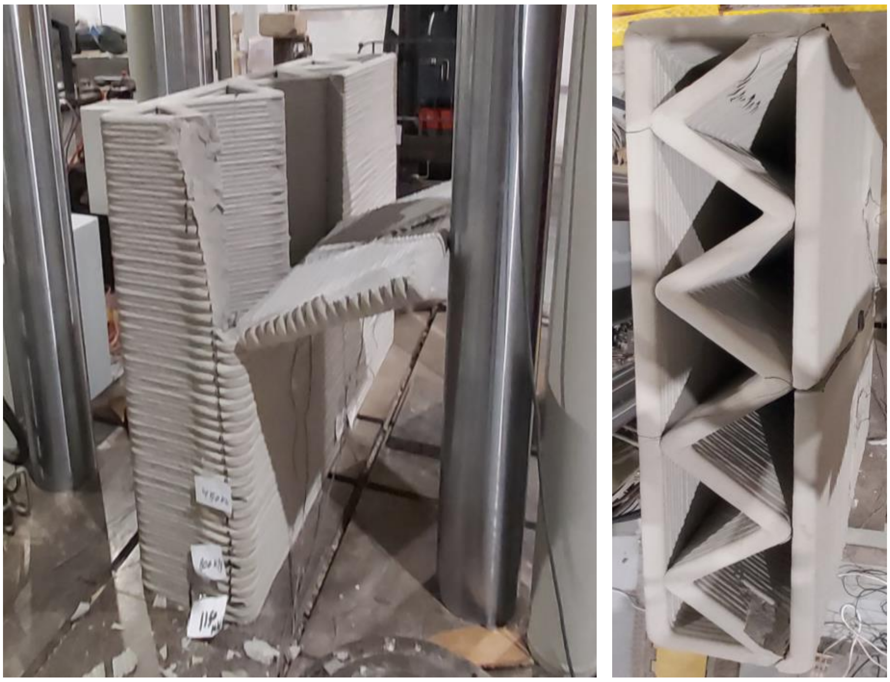

(c) GLBW-4T cross-section and wall appearance after testing.

Figure 4.13 GLBW-4T Cracks and failure patterns.

4.3.3 GLBW-5T Load Bearing Wall Testing

The load-bearing test was conducted for the LBW-5T wall, configured with five triangles in the inner zone and an increased number of truss members to 10 elements, as illustrated in Figure 4.14. The results were presented graphically as load-displacement relationships, with the machine recording a maximum vertical displacement of 6 mm, corresponding to a load bearing of 1612 kN as shown in Figure 4.15-a.

Figure 4.14 GLBW-5T Dimensions and Configuration

Figure 4.15-b shows the maximum recorded vertical displacement of 1.77 mm, and the maximum lateral displacement reached 1.78 mm at 1498 kN before the LVDTs were removed due to safety concerns following successive vertical and transverse cracks. The installed strain gauges shown in Figure 4.15-c recorded strain in both vertical and horizontal directions on both faces of the walls, with readings fluctuating due to sensitivity and sudden movements during cracking. The maximum compressive strain recorded by strain-gauge#2 was 162 μm/mm, while the maximum tensile strain by strain gauge strain-gauge #1 was 83 μm/mm, corresponding to loads of 528 kN and 537 kN, respectively.

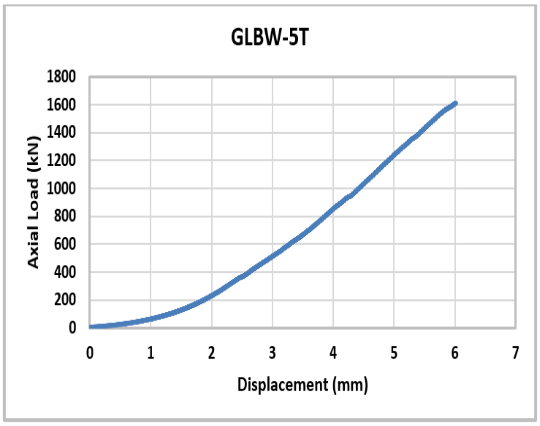

(a) Load-displacement relationship

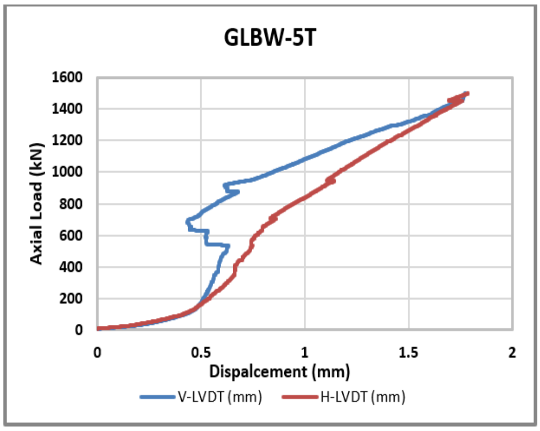

(b) Load vs deflection and buckling.

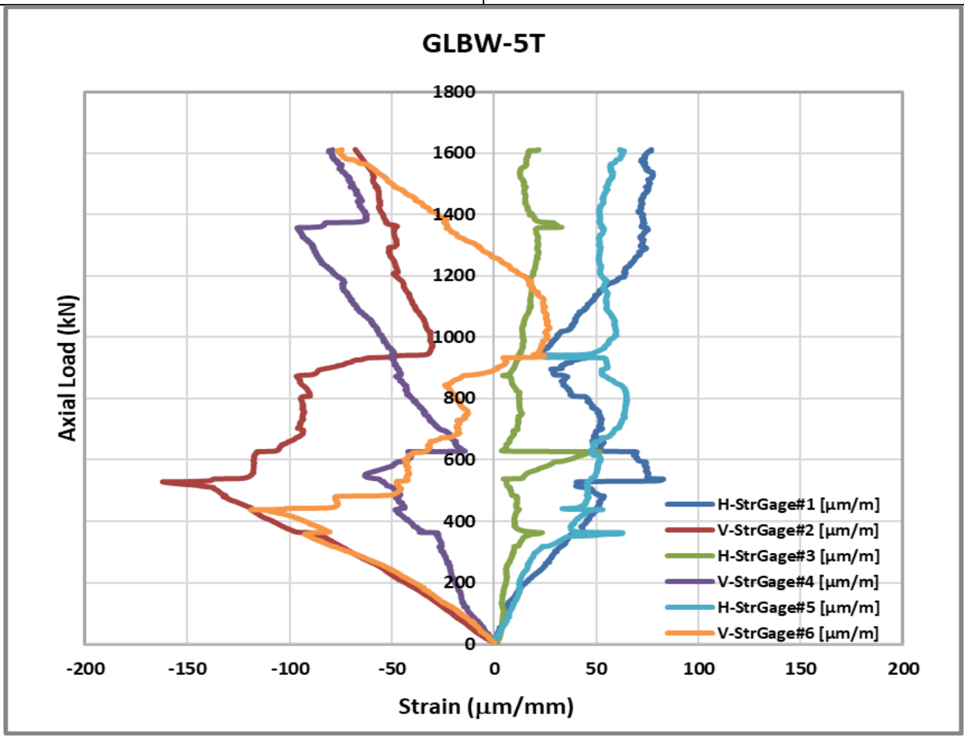

(c) Vertical and Horizontal strain gauges results.

Figure 4.15 GLBW-5T Testing Results

The observed crack widths measured 4 mm on the backside and 6 mm on the left side at a load of 1450 kN. Despite exhibiting a maximum load capacity of 1612 kN, the test was halted due to safety concerns, indicating the wall specimen's ability to withstand loads exceeding 1612 kN. In the case of the GLBW-5T wall specimen, the first crack appeared at a load of 380 kN, followed by vertical propagation from top to bottom at the front side presented in Figure 4.16-a. Subsequently, transverse cracks occurred on the left side at a load of 1350 kN after the initiation of the vertical crack at 950 kN

Figure 4.16-b. Vertical cracks appeared on the right side at 740 kN, followed by a transverse crack at 1430 kN Figure 4.16-b. Notably, the wall experienced more cracks compared to previous walls, resulting in its collapse into segments after the removal of the top steel beam Figure 4.16-c. No visible horizontal cracks were observed at the interface between printed layers during the test, except for the split part.

(a) First crack @ 380 kN

(b) Vertical and transfer cracks along the wall's sides

(c) GLBW-5T cross-section and wall appearance after testing.

Figure 4.16 GLBW-5T Cracks and failure patterns.

4.3.4 SLBW Load Bearing Wall Testing

The load-bearing test was conducted for the SLBW wall to determine its load-bearing capacity. This wall features a solid cross-section with no gaps in the inner zone Figure 4.17. Results were graphically presented as load-displacement relationships, with the machine recording a maximum vertical displacement of 3 mm, corresponding to a load-bearing capacity of 2034 kN as presented in Figure 4.18-a.

Figure 4.17 SLBW Dimensions and Configuration

According to the LVDTs readings, the maximum recorded vertical displacement was 0.96 mm, and the maximum lateral displacement reached 0.42 mm at loads of 2033.7 kN and 1223.4 kN, respectively which is shown in Figure 4.18-b. The strain gauges were installed in both vertical and horizontal directions on both faces of the walls, and strain results are presented in Figure 4.18-c. Strain gauges # 1, 3 & 5 were placed horizontally to record tensile strain, with #1 & 3 transitioning from tension to compression zones after the first crack, while #5 recorded a maximum tensile strain of 112 μm/mm at 1391 kN. Vertically, strain gauges recorded compressive strain, with #2 recording the maximum value of 433 μm/mm at 1462 kN. Only strain gauge #4 changed from compression to tension at a high load of 1500 kN indicating no obvious vertical buckling on the wall surface.

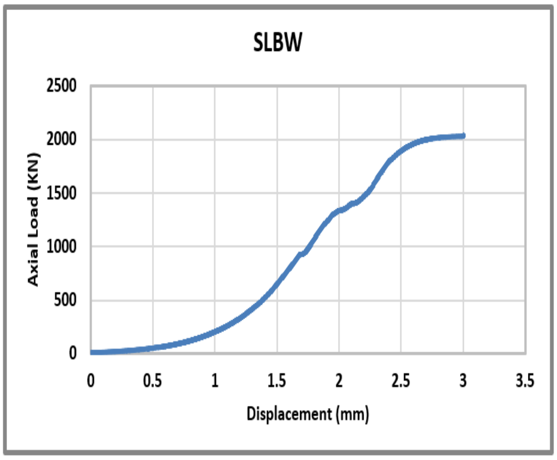

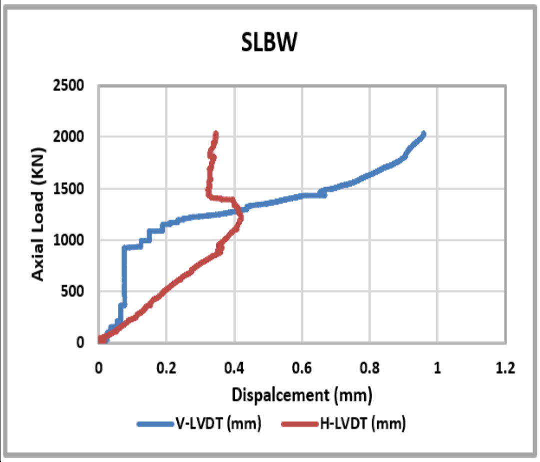

(a) **Load-displacement relationship**

(b) **Load vs deflection and buckling.**

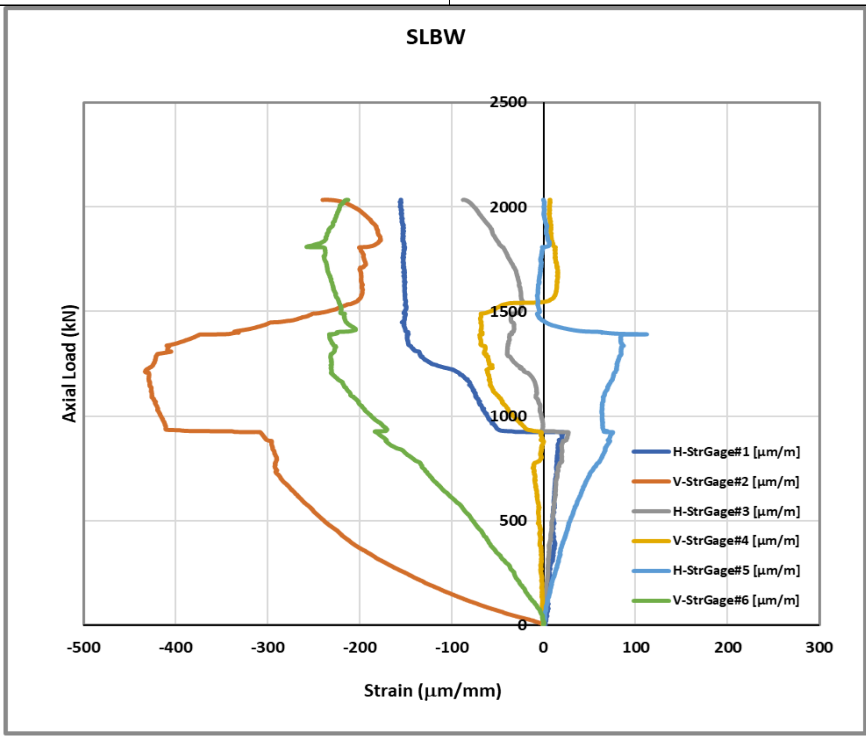

(c) **Vertical and Horizontal strain gauges results.**

Figure 4.18 SLBW Testing Results

In the case of the SLBW wall specimen, the first crack appeared at a load of 925 kN Figure 4.19-a, followed by vertical propagation from the top to the bottom at the front side. Transverse cracks then occurred at the bottom, associated with a load of 1400 kN. Similarly, on the backside, a vertical crack appeared at 1287 kN, followed by a transverse crack at 1450 kN. Additionally, on the right side of the wall, a vertical crack occurred at a load of 1150 kN Figure 4.19-b, followed by a transverse crack at 1660 kN. The observed maximum crack width was 3.2 mm on the front side of the wall, measured at a load of 1950 kN. The wall specimen exhibited a maximum load capacity of 2034 kN, and LVDTs were not removed during the test as no serious failure was observed as shown in Figure 4.19-c. It's important to note that the number of cracks on this wall is less compared to previous walls, resulting in the integration of the wall after the removal of the top steel beam. No visible horizontal cracks were observed at the interface between printed layers during or after the test.

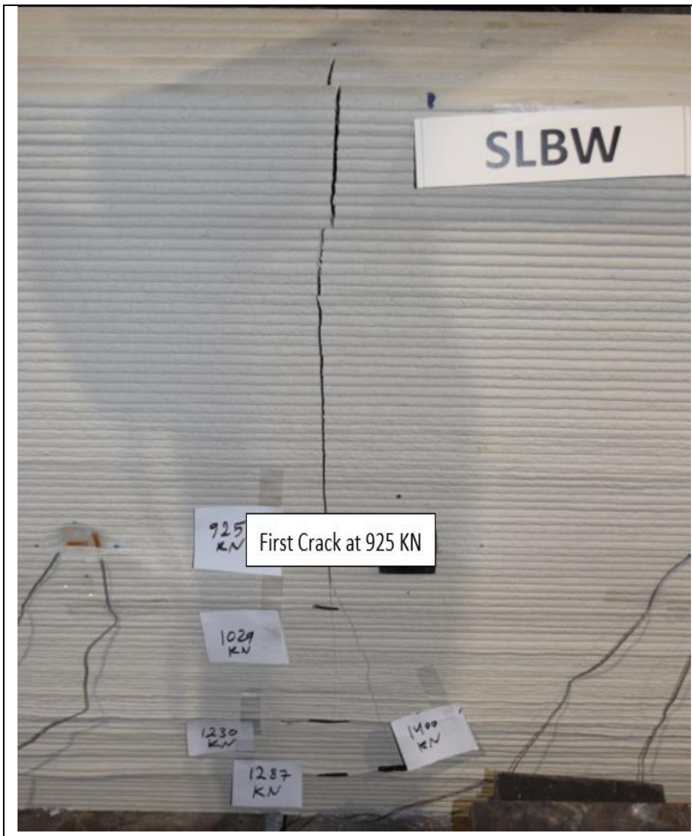

(a) First crack @ 925 kN

(b) Vertical and transfer cracks along the wall's sides

(c) GLBW-5T cross-section and wall appearance after testing.

Figure 4.19 SLBW Cracks and Failure Patterns.

4.4 The Overall Structural Performance of 3DPC Load-Bearing Walls

Table 4-3 Structural Performance Summary Of The Tested Walls.

Specimen / Evaluation	GLBW-3T	GLBW-4T	GLBW-5T	SLBW
Cross-section Configuration	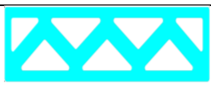	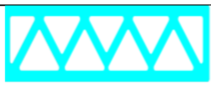	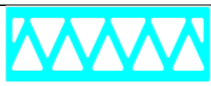	
Wall Size (mm)	1150 x 800 x 250	1150 x 800 x 250	1150 x 800 x 250	1150 x 800 x 250
Area m^2	0.18050	0.14884	0.1564	0.2875
Area %	62.8	51.8	54.4	100
Volume m^3	0.1444	0.11907	0.12514	0.23
Wall Printing Time (min)	77	63	67	122
Cracking Load (kN)	450	295	380	925
Max-Load (kN)	1516	1704	1612	2034
Max-Crack Width (mm)	3.6	9.6	6	3.2
Max Buckling (mm)	1.5	1.77	1.78	0.42
Max-V-Displacement (mm)	1.7	1.72	1.77	0.96
Max tensile strain (μm/mm)	281.4	92	83	156
Max compressive strain (μm/mm)	173	160.7	162.2	433
Cracking Intensity	Moderate intensity of cracking	Intense in cracking	Very intense in cracking	Low number of cracks
Element Rigidity after Testing	Remained rigid	Partially fall in part	Fall in parts	Remained rigid.

The performance of each wall type, as indicated by the provided data in Table 4.3, reveals distinct characteristics and outcomes. GLBW-3T, including approximately 62.8% of the total cross-sectional area, demonstrated moderate cracking intensity with a maximum crack width of 3.6 mm. Despite reaching a maximum load of 1516 kN, it remained rigid after testing, indicating satisfactory structural integrity and it can resist a higher load than the terminated one. In contrast, GLBW-4T, occupying 51.8% of the cross-sectional area, exhibited a higher cracking intensity with a notable maximum crack width of 9.6 mm. Although it tolerated a substantial maximum load of 1704 kN, the wall only partially retained its structure post-testing. GLBW-5T, with a cross-sectional area of 45.4%, showcased a similar high cracking intensity and substantial crack width of 6 mm. Despite achieving a maximum load of 1612 kN, the wall filled into segments after testing. In comparison, SLBW, constituting the entire cross-sectional area, demonstrated superior performance. With a first cracking load of 925 kN and a maximum load of 2034 kN, it exhibited minimal cracking with a maximum width of 3.2 mm, and importantly, it remained rigid post-testing. This highlights SLBW's resilience and structural stability, suggesting its suitability for load-bearing applications.

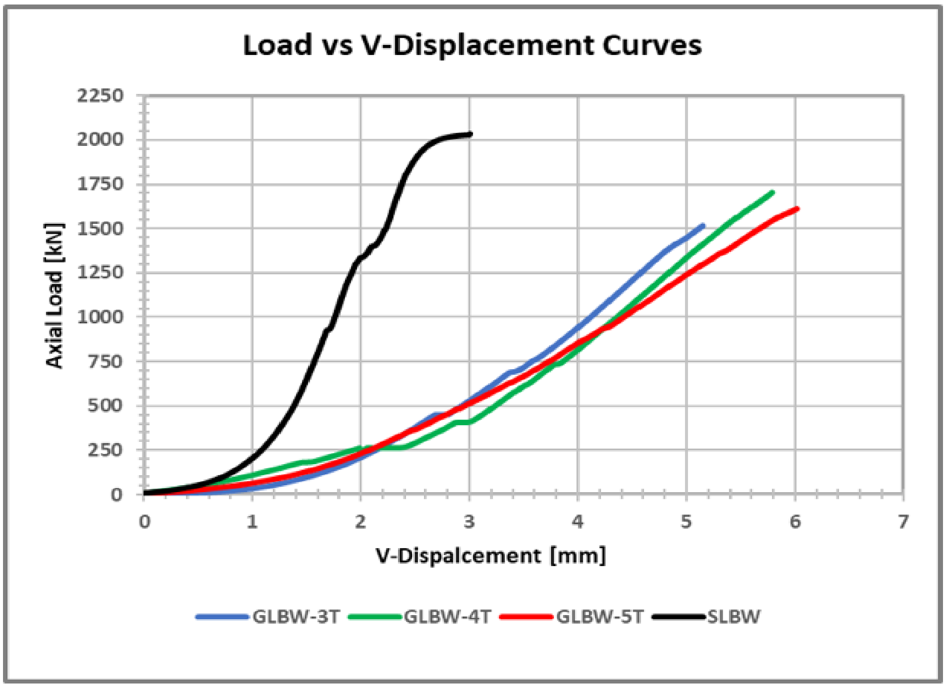

Figure 4.20 Walls Load-Displacement Comparison.

The graph in Figure 4.20 illustrates the behavior of the walls by plotting the applied load against the vertical displacement induced by the machine. Among the three gaped walls identified as GLBW, a similar load-displacement trend is evident, although with variations in crack initiation and patterns. In contrast, the solid wall (SLBW) demonstrates a rigid performance, exhibiting high resistance to vertical deformation under the applied load. SLBW also exhibits the highest stiffness and minimal deformation. Additionally, the walls' failure mode appears to be brittle, as indicated by the lack of yielding and consistent with the mechanical testing results discussed earlier.

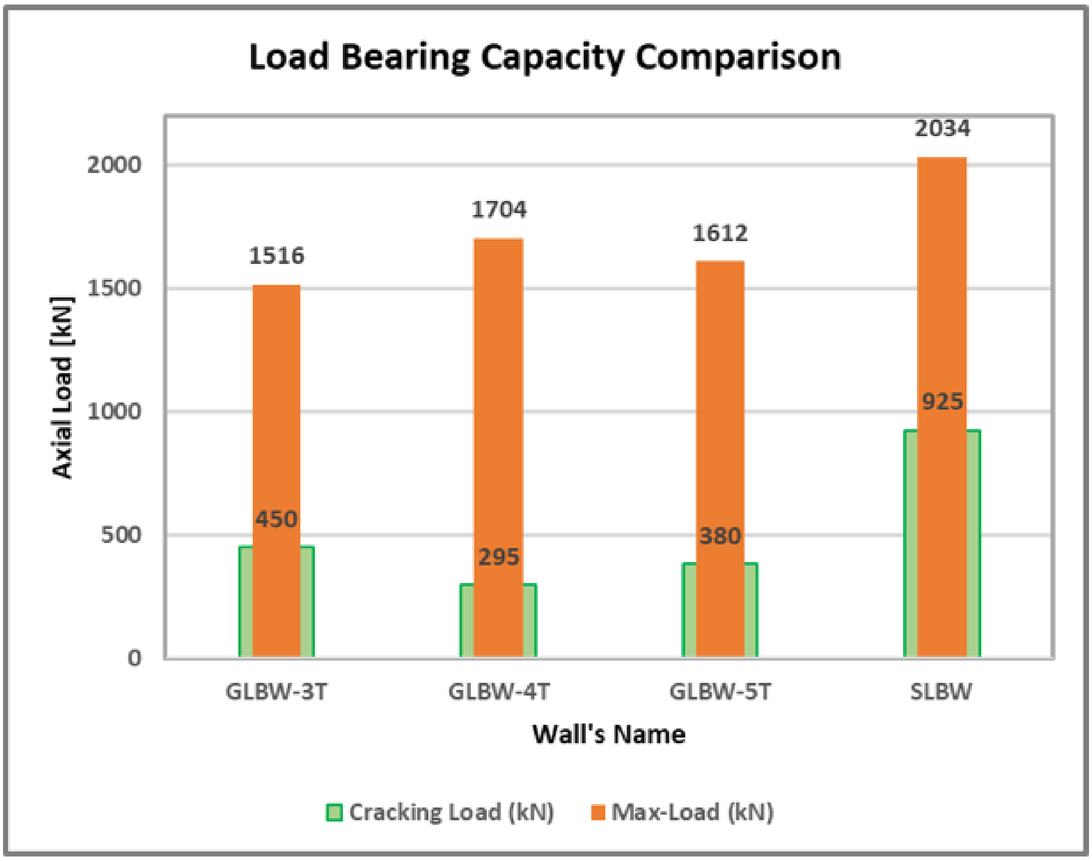

Figure 4.21 Load Bearing Capacity Comparison

Additionally, based on the data presented in Figure 4.21, SLBW displayed the highest crack load resistance at 925 kN, followed by GLBW-3T at 450 kN, surpassing GLBW-4T and GLBW-5T with crack loads of 295 kN and 380 kN, respectively. A higher crack load resistance typically correlates with better overall wall or structural performance. Interestingly, despite GLBW-3T having fewer truss members in the core zone compared to GLBW-4T and GLBW-5T, it exhibited higher crack load resistance. This could be attributed to the doubled adjacent printed layers in the core zone of GLBW-3T, in contrast to single layers in GLBW-4T and GLBW-5T. The doubled layers in GLBW-3T contributed to increased bearing load capacity and structural stability, resulting in lower crack intensity and fewer crack patterns. Additionally, considering the maximum bearing load for each wall, SLBW demonstrated the highest load at 2034 kN, followed by GLBW-4T at 1704 kN, and GLBW-5T and GLBW-3T at loads of 1612 kN and 1516 kN, respectively.

Furthermore, material consumption is an important issue to be considered for optimal and economical efficiency. The first cracking load was also considered as it serves as a key indicator of the structural performance against the initial observed failure. Based on Figure 4.22, which illustrates the relationship between the material quantities and the cracking load for each wall. The first cracking load resistance increased as the volume increased. Also, It is evident that the SLBW achieved the highest resisting capacity to the cracking load such that the crack load to the volume ratio is 4.02 N/cm^3, however, it consumed the highest amount of printed material at 0.230 m^3. In contrast, GLBW-3T and GLBW-5T, both gapped load-bearing walls with varying truss configurations, demonstrated nearly similar efficiency ratios, with crack load-to-volume ratios of 3.12 N/cm^3 and 3.04 N/cm^3, respectively. This indicates that these configurations, while consuming less material than the SLBW, still maintained a relatively high resistance to cracking. On the other hand, GLBW-4T showed the least efficient performance with a crack load-to-volume ratio of 2.48 N/cm^3, indicating that it consumed more material relative to its cracking load resistance compared to the other configurations.

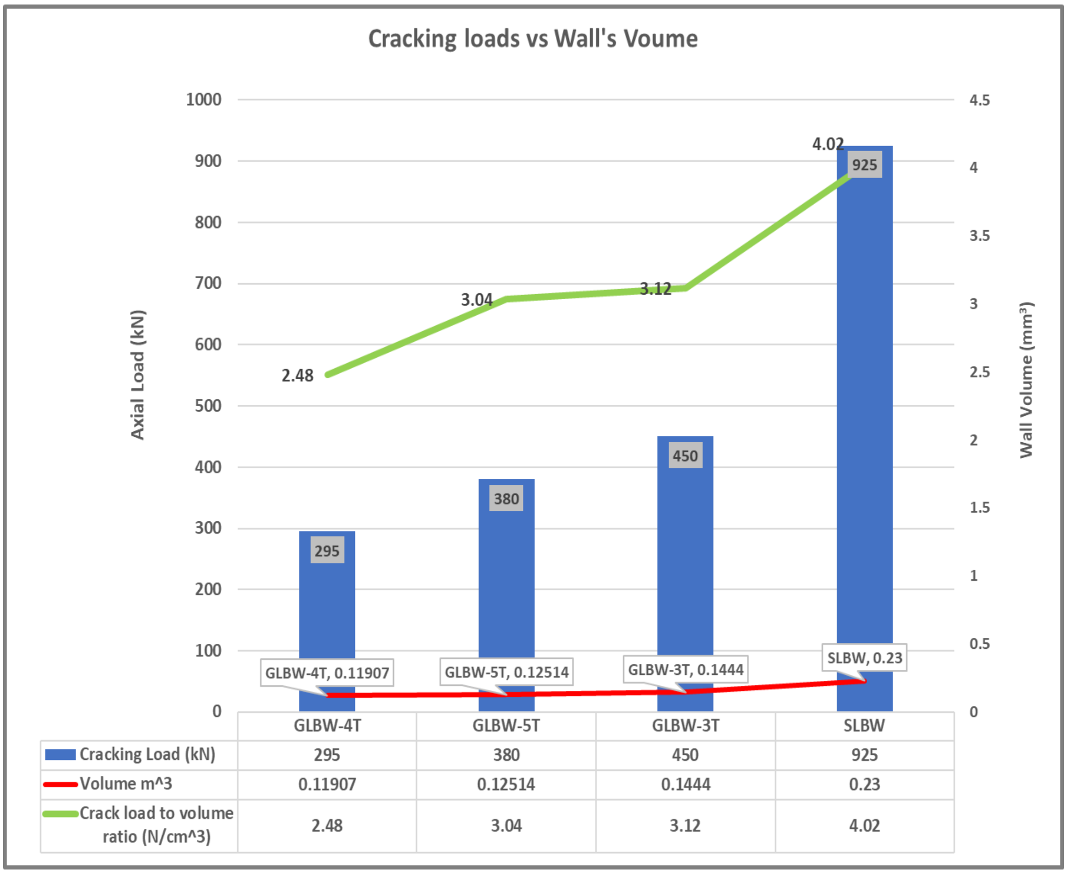

Figure 4.22 Walls Volume Correlation To The Cracking Loads.

Moreover, Figure 4.23 depicts a bar chart illustrating deformation data, including maximum vertical displacement, maximum lateral (buckling) displacement, and maximum crack width. These parameters were observed and recorded at the termination of the tests for each wall specimen. The gapped walls (3T, 4T, and 5T) exhibited nearly identical maximum vertical displacements of 1.7 mm, whereas the SLBW demonstrated the least vertical deformation at 0.96 mm. Similarly, concerning lateral displacement, the gapped walls (3T & 4T) showed the highest maximum buckling of 1.77 mm and 1.78 mm, respectively, with GLBW-3T recording a slightly lower value of 1.5 mm. Conversely, the SLBW exhibited the lowest buckling value at 0.42 mm due to its high wall stability. Finally, the maximum crack width was monitored using a crack meter sensor at the end of the testing. GLBW-4T displayed the widest crack width at approximately 9.6 mm, followed by GLBW-5T at 6 mm, while GLBW-3T and SLBW achieved similar crack widths at 3.6 mm and 3.2 mm, respectively. This underscores that GLBW-3T demonstrated superior structural performance with fewer cracks, narrower crack widths, and lower quantities of printed mortar, representing 62.8% of SLBW, thus highlighting the optimal structural performance and material savings associated with GLBW-3T.

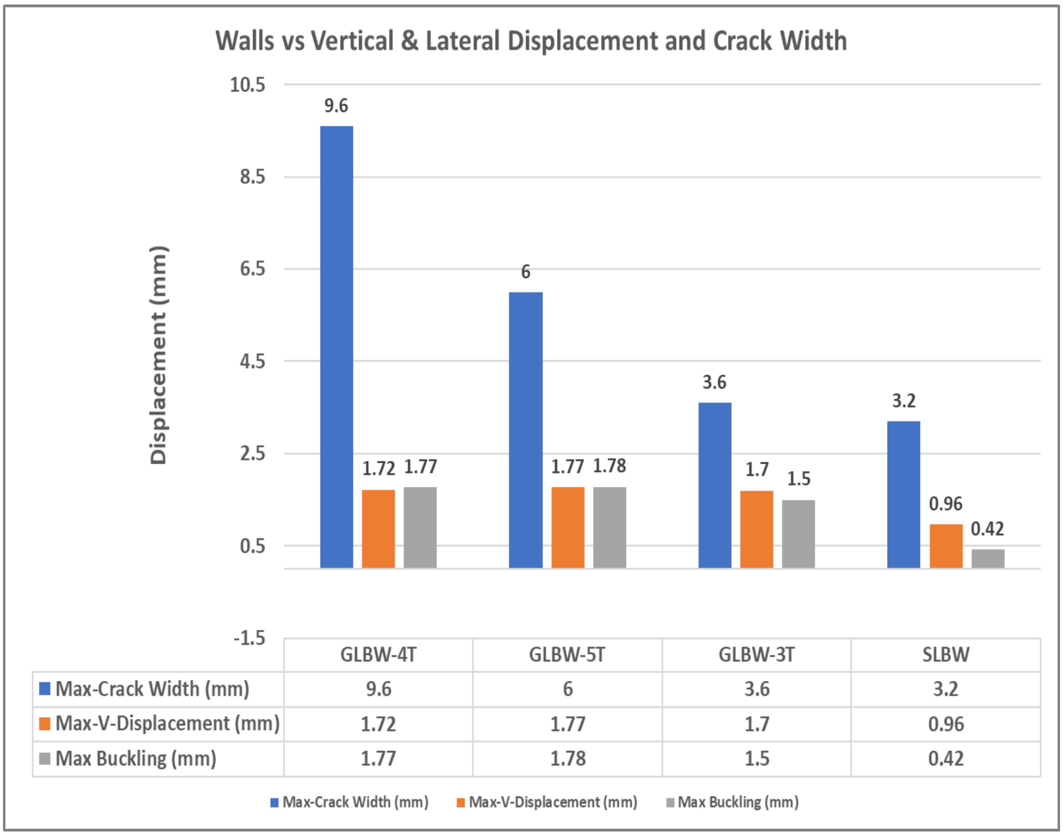

Figure 4.23 Walls Max Displacements and Crack Width

Chapter 5. Conclusion and Recommendations

5.1 Conclusion

3D Concrete Printing (3DCP) holds significant promise for revolutionizing the future of construction. Thus, the study of the structural performance of 3DCP is imperative for assessing its feasibility and reliability in construction applications. Understanding how 3DCP elements behave under various loading conditions provides valuable insights into their strength, stability, and durability by evaluating factors such as load-bearing capacity, deformation characteristics, and failure modes. Ultimately, such investigations contribute to the advancement of 3DCP technology and its integration into mainstream construction practices.

This study evaluated the load-bearing capacity and structural performance of 3D-printed concrete walls with varying cross-section geometries, namely GLBW-3T, GLBW-4T, GLBW-5T, and SLBW. By increasingly altering the number of truss members, it has aimed to understand their direct impact on load-bearing behavior. The findings revealed that the cross-section patterns significantly influence stress distribution, load transfer paths, cracks patterns and cracks intensity, and ductility, highlighting the critical role of the inner truss in the bracing system to prevent buckling failure. Additionally, this study assessed the rheological properties of the concrete mix to ensure consistency, workability, and buildability, thereby minimizing cracking and extrusion discontinuity. Also, Experimental investigations focused on the mechanical properties, including compressive, flexural, and tensile strength characteristics. The following conclusions can be drawn from this research:

- The 7-day compressive strength assessment revealed an average value of 85 MPa for cast samples, while printed samples exhibited average strengths of 58 MPa, 48 MPa, and 40 MPa in directions perpendicular, longitudinal, and parallel to the printed layers, respectively.
- Notably, the anisotropic nature of the mortar, attributed to the presence of glass fibers acting as material composite-like. Furthermore, the layer-by-layer printing process results in orthotropic behavior due to contact areas along the interfaces of printed layers.
- Flexural tests revealed that cast concrete prisms had an average strength of 12.3 MPa. While, the printed prisms showed average strengths of 11.8 MPa in the N

direction and 10.4 MPa in the P direction, achieving 96% and 85% of the cast prism's flexural strength, respectively.

- The SLBW, designed as a control large-scale sample representing 100% of the cross-sectional area, exhibited the highest capacity against the first crack load, recording 925 kN.
- The gaped section walls (GLBWs) showed comparatively lower structural performance, with GLBW-3T exhibiting the highest crack load resistance at 450 kN, due to its doubled layer core zone, while GLBW-4T displayed the lowest crack load.
- The maximum load-bearing capacity was highest for SLBW at 2034 kN, followed by GLBW-4T at 1704 kN, GLBW-5T at 1612 kN, and GLBW-3T at 1516 kN.
- The evaluation of structural performance indicated that SLBW and GLBW-3T performed the best in terms of crack intensity and patterns, whereas GLBW-5T showed the poorest performance due to increased truss tips resulting in multi-directional cracking.
- The observed failure mode across all walls was predominantly brittle. SLBW and GLBW-3T were capable of resisting higher loads beyond the recorded values, unlike GLBW-4T and GLBW-5T, which experienced partial and full collapses, respectively.

5.2 Recommendations

Based on the research conducted and the findings presented in this study, the following suggestions may offer valuable guidance for future investigations in the field of 3D-printed concrete structural walls:

- Investigate the use of different types of fibers or additives to enhance the mechanical properties and structural performance of 3D-printed concrete walls.
- Conduct long-term durability studies to assess the performance of 3D-printed concrete walls under various environmental conditions, including exposure to moisture, freeze-thaw cycles, and chemical exposure.
- Explore the integration of smart sensors into 3D-printed concrete walls for real-time structural health monitoring, providing early warnings of potential issues

like cracking or deformation. Additionally, consider the use of 3D Digital Image Correlation (DIC) Systems for accurate crack width measurement.

- Explore the addition of vertical and horizontal reinforcement within the printed concrete walls to enhance their structural integrity and resistance to lateral loads, such as wind or seismic forces.
- Conduct FEM analysis to simulate the behavior of 3D-printed concrete walls under various loading conditions, including axial, lateral, and impact loads. This analysis will provide insights into the structural response, deformation patterns, and stress distribution within the walls, allowing for optimization of design parameters and reinforcement layouts.

References

[1] G. MA and L. WANG, “A critical review of preparation design and workability measurement of concrete material for largescale 3D printing,” vol. 12, no. 3, pp. 382–400, Sep. 2018, doi: 10.1007/s11709-017-0430-x.

[2] R. Comminal, W. R. Leal da Silva, T. J. Andersen, H. Stang, and J. Spangenberg, “Modelling of 3D concrete printing based on computational fluid dynamics,” vol. 138, p. 106256, Dec. 2020, doi: 10.1016/j.cemconres.2020.106256.

[3] L. Gebhard, J. Mata-Falcón, A. Anton, B. Dillenburger, and W. Kaufmann, “Structural behaviour of 3D printed concrete beams with various reinforcement strategies,” vol. 240, p. 112380, Aug. 2021, doi: 10.1016/j.engstruct.2021.112380.

[4] X. Han, J. Yan, M. Liu, L. Huo, and J. Li, “Experimental study on large-scale 3D printed concrete walls under axial compression,” vol. 133, p. 103993, Jan. 2022, doi: 10.1016/j.autcon.2021.103993.

[5] V. Mechtcherine, V. N. Nerella, F. Will, M. Näther, J. Otto, and M. Krause, “Large-scale digital concrete construction – CONPrint3D concept for on-site, monolithic 3D-printing,” vol. 107, p. 102933, Nov. 2019, doi: 10.1016/j.autcon.2019.102933.

[6] R. A. Buswell, W. R. Leal de Silva, S. Z. Jones, and J. Dirrenberger, “3D printing using concrete extrusion: A roadmap for research,” vol. 112, pp. 37–49, Oct. 2018, doi: 10.1016/j.cemconres.2018.05.006.

[7] M. Alabbasi, A. Agkathidis, and H. Chen, “Robotic 3D printing of concrete building components for residential buildings in Saudi Arabia,” vol. 148, p. 104751, Apr. 2023, doi: 10.1016/j.autcon.2023.104751.

[8] D. Marchon, S. Kawashima, H. Bessaies-Bey, S. Mantellato, and S. Ng, “Hydration and rheology control of concrete for digital fabrication: Potential admixtures and cement chemistry,” vol. 112, pp. 96–110, Oct. 2018, doi: 10.1016/j.cemconres.2018.05.014.

[9] T. T. Le, S. A. Austin, S. Lim, R. A. Buswell, A. G. F. Gibb, and T. Thorpe, “Mix design and fresh properties for high-performance printing concrete,” vol. 45, no. 8, pp. 1221–1232, Aug. 2012, doi: 10.1617/s11527-012-9828-z.

[10] B. Panda, C. Unluer, and M. J. Tan, “Investigation of the rheology and strength of geopolymer mixtures for extrusion-based 3D printing,” vol. 94, pp. 307–314,

Nov. 2018, doi: 10.1016/j.cemconcomp.2018.10.002.

[11] B. Panda, S. Ruan, C. Unluer, and M. J. Tan, “Improving the 3D printability of high volume fly ash mixtures via the use of nano attapulgite clay,” vol. 165, pp. 75–83, May 2019, doi: 10.1016/j.compositesb.2018.11.109.

[12] J. G. Sanjayan, R. Jayathilakage, and P. Rajeev, “Vibration induced active rheology control for 3D concrete printing,” vol. 140, p. 106293, Feb. 2021, doi: 10.1016/j.cemconres.2020.106293.

[13] B. Khoshnevis, “Robotic systems for automated construction,” Nov. 08, 2013.

[14] H. Kwon, “Experimentation and analysis of contour crafting (CC) process using uncured ceramic materials.” University of Southern California Digital Library (USC.DL), Jan. 01, 2016, [Online].Available: https://explore.openaire.eu/search/dataset?datasetId=datacite____::076a0d96ef abaa5d9d57e0131f832642.

[15] M. S. Khan, F. Sanchez, and H. Zhou, “3-D printing of concrete: Beyond horizons,” vol. 133, p. 106070, Jul. 2020, doi: 10.1016/j.cemconres.2020.106070.

[16] J. Pegna, “Exploratory investigation of solid freeform construction,” vol. 5, no. 5, pp. 427–437, 1997, doi: 10.1016/S0926-5805(96)00166-5.

[17] A. Kazemian, X. Yuan, E. Cochran, and B. Khoshnevis, “Cementitious materials for construction-scale 3D printing: Laboratory testing of fresh printing mixture,” vol. 145, pp. 639–647, Aug. 2017, doi: 10.1016/j.conbuildmat.2017.04.015.

[18] J. B. Gardiner, “Exploring the Emerging Design Territory of Construction 3D Printing – Project Led Architectural Research.” Unpublished, Jan. 01, 2011, doi: 10.13140/rg.2.2.11676.28807.

[19] R. A. Buswell, R. C. Soar, A. G. F. Gibb, and A. Thorpe, “Freeform Construction: Mega-scale Rapid Manufacturing for construction,” vol. 16, no. 2, pp. 224–231, Mar. 2007, doi: 10.1016/j.autcon.2006.05.002.

[20] X. Zhang et al., “Large-scale 3D printing by a team of mobile robots,” vol. 95, pp. 98–106, Nov. 2018, doi: 10.1016/j.autcon.2018.08.004.

[21] F. Bos, R. Wolfs, Z. Ahmed, and T. Salet, “Additive manufacturing of concrete in construction: potentials and challenges of 3D concrete printing,” vol. 11, no. 3, pp. 209–225, Jul. 2016, doi: 10.1080/17452759.2016.1209867.

[22] C. Gosselin, R. Duballet, P. Roux, N. Gaudillière, J. Dirrenberger, and P. Morel, “Large-scale 3D printing of ultra-high performance concrete – a new processing

route for architects and builders," vol. 100, pp. 102–109, Jun. 2016, doi: 10.1016/j.matdes.2016.03.097.

[23] H. Al Jassmi, F. Al Najjar, and A.-H. I. Mourad, "Large-Scale 3D Printing: The Way Forward," vol. 324, no. 1, p. 12088, Mar. 2018, doi: 10.1088/1757-899X/324/1/012088.

[24] A. S. J. Suiker, "Mechanical performance of wall structures in 3D printing processes: Theory, design tools and experiments," vol. 137, pp. 145–170, Mar. 2018, doi: 10.1016/j.ijmecsci.2018.01.010.

[25] O. Kontovourkis and G. Tryfonos, "Robotic 3D clay printing of prefabricated non-conventional wall components based on a parametric-integrated design," vol. 110, p. 103005, Feb. 2020, doi: 10.1016/j.autcon.2019.103005.

[26] V. Nguyen-Van, H. Nguyen-Xuan, B. Panda, and P. Tran, "3D concrete printing modelling of thin-walled structures," vol. 39, pp. 496–511, May 2022, doi: 10.1016/j.istruc.2022.03.049.

[27] T. Daungwilailuk, P. Pheinsusom, and W. Pansuk, "Uniaxial load testing of large-scale 3D-printed concrete wall and finite-element model analysis," vol. 275, p. 122039, Mar. 2021, doi: 10.1016/j.conbuildmat.2020.122039.

[28] G. Tanapornraweekit, P. Jiramarootapong, S. Paudel, S. Tangtermsirikul, and C. Snguanyat, "Experimental and numerical investigation of 3D-printed mortar walls under uniform axial compression," vol. 360, p. 129552, Dec. 2022, doi: 10.1016/j.conbuildmat.2022.129552.

[29] L. Pham, P. Tran, and J. Sanjayan, "Steel fibres reinforced 3D printed concrete: Influence of fibre sizes on mechanical performance," vol. 250, p. 118785, Jul. 2020, doi: 10.1016/j.conbuildmat.2020.118785.

[30] ASTM, "ASTM C143 - Standard Test Method for Slump of Hydraulic-Cement Concrete," ASTM International, West Conshohocken, PA, 2015, DOI: 10.1520/C0143-15A.

[31] ASTM, "ASTM C1611 - Standard Test Method for Slump Flow of Self-Consolidating Concrete," ASTM International, West Conshohocken, PA, 2017, DOI: 10.1520/C1611_C1611M-17.

[32] G. H. Ahmed, N. H. Askandar, and G. B. Jumaa, "A review of largescale 3DCP: Material characteristics, mix design, printing process, and reinforcement strategies," vol. 43, pp. 508–532, Sep. 2022, doi: 10.1016/j.istruc.2022.06.068.

[33] ASTM, "ASTM C191-04 - Standard Test Methods for Time of Setting of

Hydraulic Cement by Vicat Needle," ASTM International, West Conshohocken, PA, 2004, DOI: 10.1520/C0191_C0191M-04.

[34] ASTM, "ASTM C109/C109M-20 - Standard Test Method for Compressive Strength of Hydraulic Cement Mortars (Using 2-in. or [50-mm] Cube Specimens)," ASTM International, West Conshohocken, PA, 2020, DOI: 10.1520/C0109_C0109M-20.

[35] International Code Council, "Acceptance Criteria for Approval of Plastic Surface Bonded Concrete," ICC-ES, Whittier, CA, USA, AC509, 2010.

[36] ASTM International, "Standard Test Method for Flexural Strength of Hydraulic-Cement Mortars," ASTM C348-19, West Conshohocken, PA, USA, 2019, doi:10.1520/C0348-19.

[37] B. Panda, S. Chandra Paul, and M. Jen Tan, "Anisotropic mechanical performance of 3D printed fiber reinforced sustainable construction material," vol. 209, pp. 146–149, Dec. 2017, doi: 10.1016/j.matlet.2017.07.123.

[38] ASTM International, "Standard Test Method for Tensile Properties of Plastics," ASTM D638-14, West Conshohocken, PA, USA, 2014. doi:10.1520/D0638-14.

Vita

Arafat A. Mohammed, born in 1992 in Ta'aiz, Republic of Yemen, completed his secondary education in Ta'aiz. He earned his B.Sc. degree in Civil and Environmental Engineering from King Faisal University, Saudi Arabia, in 2017. From 2017 to 2021, he worked as a Civil Engineer in various companies in Saudi Arabia and Yemen, including Masheed Elengaz est., Saeed Bakhroosh Co., Saudi Coasts Co., and IOM org. In January 2022, he joined the Civil Engineering master's program at the American University of Sharjah as a graduate teaching and research assistant. His research interests include additive manufacturing construction, pre-engineered steel buildings, and biological wastewater treatment.